RESEARCH ARTICLE

SIRT5 Is a Druggable Metabolic Vulnerability in Acute Myeloid Leukemia

Dongqing Yan[1], Anca Franzini[1], Anthony D. Pomicter[1], Brayden J. Halverson[1], Orlando Antelope[1], Clinton C. Mason[2], Jonathan M. Ahmann[1], Anna V. Senina[1], Nadeem A. Vellore[1], Courtney L. Jones[3], Matthew S. Zabriskie[1], Hein Than[4], Michael J. Xiao[1], Alexandria van Scoyk[1], Ami B. Patel[5], Phillip M. Clair[1], William L. Heaton[1], Shawn C. Owen[6], Joshua L. Andersen[7], Christina M. Egbert[7], Julie A. Reisz[8], Angelo D'Alessandro[3,8], James E. Cox[9], Kevin C. Gantz[1], Hannah M. Redwine[1], Siddharth M. Iyer[1], Jamshid S. Khorashad[10], Nima Rajabi[11], Christian A. Olsen[11], Thomas O'Hare[1,5], and Michael W. Deininger[1,5]

ABSTRACT We discovered that the survival and growth of many primary acute myeloid leukemia (AML) samples and cell lines, but not normal CD34+ cells, are dependent on SIRT5, a lysine deacylase implicated in regulating multiple metabolic pathways. Dependence on SIRT5 is genotype agnostic and extends to RAS- and p53-mutated AML. Results were comparable between SIRT5 knockdown and SIRT5 inhibition using NRD167, a potent and selective SIRT5 inhibitor. Apoptosis induced by SIRT5 disruption is preceded by reductions in oxidative phosphorylation and glutamine utilization, and an increase in mitochondrial superoxide that is attenuated by ectopic superoxide dismutase 2. These data indicate that SIRT5 controls and coordinates several key metabolic pathways in AML and implicate SIRT5 as a vulnerability in AML.

SIGNIFICANCE: Reducing SIRT5 activity is detrimental to the survival of AML cells regardless of genotype, yet well tolerated by healthy hematopoietic cells. In mouse models, disrupting SIRT5 inhibits AML progression. SIRT5 controls several metabolic pathways that are required for leukemia cell survival. These results identify SIRT5 as a therapeutic target in AML.

See related commentary by Li and Melnick, p. 198.

INTRODUCTION

Acute myeloid leukemia (AML) is a genetically heterogeneous myeloid neoplasm with poor prognosis (1). With the exception of acute promyelocytic leukemia, standard therapy for AML remained unchanged for three decades, consisting of induction with anthracycline and cytarabine, followed by consolidation with high-dose cytarabine or bone marrow (BM) transplant (1–4). Despite high rates of complete response (CR) to initial chemotherapy, most patients relapse and eventually succumb to AML, suggesting that chemotherapy eliminates AML blasts, but not leukemia-initiating cells (LIC) that survive in the protective microenvironment of hematopoietic organs (5). Recently, therapy options have been enriched by inhibitors of FLT3 or mutant isocitrate dehydrogenase 1/2 (IDH1/2), validating the paradigm of genotype-directed therapy (6–9). Unfortunately, even with these new drugs, relapse is common and frequent due to selection of subclones with resistance mutations in the drug target (7, 10–12). Unlike FLT3 and IDH1/2 inhibitors, the BCL2 inhibitor venetoclax is active in multiple AML genotypes, indicating that targeting shared vulnerabilities in a genotype-agnostic manner can be effective (11, 13). However, many venetoclax-induced responses are not durable, as leukemia cells adapt by activating alternative antiapoptosis signaling or by reprogramming mitochondrial metabolism (14, 15). Thus, microenvironmental protection, intratumoral heterogeneity and metabolic flexibility limit the utility of current AML therapeutics.

Metabolic aberrancies are increasingly recognized as potential cancer therapy targets (16). One well-established example is elevated glycolytic flux despite adequate oxygen availability, which generates intermediates to sustain nucleic acid and protein biosynthesis in rapidly dividing cells, known as the Warburg effect (17, 18). Metabolic bottlenecks in AML include oxidative phosphorylation (OXPHOS), mitochondrial creatine kinase, branched-chain amino acid aminotransferase, glutaminase (GLS), the pentose phosphate pathway, and mitochondrial translation (19–26). While some dependencies are associated with specific genotypes such as GLS with FLT3 internal tandem duplications (ITD; refs. 24, 27), others are genotype agnostic or linked to cellular subsets such as quiescent LICs, suggesting that diverse genotypes can share metabolic vulnerabilities (28). The utility of targeting single metabolic pathways such as glycolysis (29) or GLS (30) is limited by the metabolic flexibility of cancer cells that allows for rapid adaptation and therapy escape (28, 31).

Sirtuins are NAD+-dependent lysine deacylases implicated in fundamental cellular processes such as senescence, DNA repair, and apoptosis (32). Posttranslational lysine acylation affects multiple protein classes, including metabolic enzymes (33). Among the seven mammalian sirtuins, sirtuin 5 (SIRT5) removes negatively charged acyl groups, specifically succinyl, malonyl, and glutaryl (34–36). Acylation is thought to occur nonenzymatically when relatively high pH and high concentration of acyl-CoA favor transfer of the acyl group to the deprotonated ε-amino group of lysines (34, 37). The

[1]Huntsman Cancer Institute, University of Utah, Salt Lake City, Utah. [2]Department of Pediatrics, University of Utah, Salt Lake City, Utah. [3]Division of Hematology, University of Colorado Anschutz Medical Campus, Aurora, Colorado. [4]Department of Haematology, Singapore General Hospital, Singapore. [5]Division of Hematology and Hematologic Malignancies, University of Utah, Salt Lake City, Utah. [6]Department of Pharmaceutics and Pharmaceutical Chemistry, University of Utah, Salt Lake City, Utah. [7]Department of Chemistry and Biochemistry, Brigham Young University, Provo, Utah. [8]Department of Biochemistry and Molecular Genetics, University of Colorado Anschutz Medical Campus, Aurora, Colorado. [9]Department of Biochemistry, University of Utah, Salt Lake City, Utah. [10]Department of Immunology and Inflammation, Imperial College London, London, United Kingdom. [11]Center for Biopharmaceuticals and Department of Drug Design and Pharmacology, Faculty of Health and Medical Sciences, University of Copenhagen, Copenhagen, Denmark.

Note: Supplementary data for this article are available at Blood Cancer Discovery Online (https://bloodcancerdiscov.aacrjournals.org/).

A. Franzini and A.D. Pomicter contributed equally to this article.

Corresponding Author: Michael W. Deininger, Huntsman Cancer Institute, University of Utah, 2000 Circle of Hope, Salt Lake City, UT 84112-5550. Phone: 801-581-6363; Fax: 801-585-0900; E-mail: Michael.Deininger@hci.utah.edu

Blood Cancer Discov 2021;2:266–87

doi: 10.1158/2643-3230.BCD-20-0168

three SIRT5-dependent deacylations occur at overlapping as well as unique lysines within substrate proteins (38). SIRT5 regulates multiple metabolic pathways, including fatty acid β-oxidation, glycolysis, ketogenesis, OXPHOS, and urea cycle (34, 35, 37, 38). In several cases, deacylation of specific lysine residues was shown to modulate enzymatic activity, mechanistically linking SIRT5 and metabolic programming (39, 40). At steady state, *Sirt5*$^{-/-}$ mice exhibit only mild metabolic abnormalities, including reduced glycolysis and ketogenesis (37, 38, 41). More severe phenotypes are observed under stress, such as increased dopaminergic neuronal damage upon challenge with 1-methyl-4-phenyl-1,2,3,6-tetrahydropyridine (MPTP) and cold intolerance upon caloric restriction (42–45). In several cases, phenotypes were attributable to SIRT5-dependent regulation of specific enzymes, such as uncoupling protein 1 in cold intolerance (43). These data indicate that SIRT5 orchestrates cellular responses to various stressors to reestablish tissue homeostasis.

We have discovered that knockdown (KD) or genetic absence of SIRT5 attenuates leukemia in multiple AML models and through several mechanisms, including oxidative stress. Inhibition of SIRT5 with NRD167, a cell-permeant SIRT5 inhibitor, impairs proliferation of AML, but not normal hematologic progenitors *ex vivo*, implicating SIRT5 as a therapy target in AML. Our data support the development of clinical SIRT5 inhibitors for the treatment of AML and other SIRT5-dependent cancers.

RESULTS

SIRT5 Is Essential for Survival of Primary AML Blasts Cultured on BM Stroma

To identify essential AML genes, we performed a cancer-focused shRNA screen on primary AML blasts freshly isolated from patients with newly diagnosed AML (83%–95% CD34$^+$; $n = 12$; Supplementary Table S1). As limited *ex vivo* growth and survival of primary AML cells hinder detection of relative shRNA abundance changes, most shRNA screens in AML have used cell lines. To enhance viability and growth, and mimic protective microenvironment effects, we cultured primary AML blasts on HS-5 human stromal cells (Supplementary Fig. S1A; ref. 46). We optimized the algorithm for identification of survival/growth-critical genes, prioritizing candidates based on at least two shRNAs targeting the same mRNA with a fold-reduction ranking in the top 2% of all scores, detected in at least two samples. Thirty-four genes met these criteria in at least two samples, and nine genes met these criteria in at least three samples. Top candidates included known AML vulnerabilities such as BCL2 and several genes not previously associated with AML (Supplementary Fig. S1B; Supplementary Table S2). We selected SIRT5 for further study based on the potential of targeting with a small-molecule inhibitor and the mild phenotype of *Sirt5*$^{-/-}$ mice (41). Results were confirmed by transducing cryopreserved cells with doxycycline-inducible versions of two *SIRT5*-targeting shRNAs from the initial screen (doxycycline-sh*SIRT5*$^{2311/2312}$; Supplementary Fig. S1C and S1D).

AML Cells Are Selectively Dependent on SIRT5

Both tumor-promoting and tumor-suppressive roles have been attributed to SIRT5 in solid tumors, depending on the specific context, but its function in hematologic malignancies is unknown (39). We infected CD34$^+$ cells from additional AML patients ($n = 25$; Supplementary Table S1) and cord blood (CB; $n = 5$) with doxycycline-sh*SIRT5*$^{2311/2312}$. *SIRT5* KD was comparable in AML (median 52.4%, range 24.7%–89.6%) and CB (median 65.9%, range 37.5%–80.1%; $P = 0.26$). *SIRT5* KD selectively reduced AML colony formation, with no effect on CB (Fig. 1A). For genetic validation, we infected BM cells from *Sirt5*$^{+/+}$ and *Sirt5*$^{-/-}$ mice with retrovirus for expression of the myeloid leukemia alleles *FLT3-ITD, MLL-AF9, RUNX1-RUNXT1/NRAS*^{G12D}, *BCR-ABL1*^{p210}, and *MPL*^{W515L}. Absence of *Sirt5* reduced colony formation by approximately 50%, 60%, 25%, 50%, and 20% respectively, compared with *Sirt5*$^{+/+}$ controls (Fig. 1B). Routine hematopoietic parameters and myeloid colony formation were comparable between *Sirt5*$^{-/-}$ mice and *Sirt5*$^{+/+}$ littermates (Fig. 1C; Supplementary Table S3). These data indicate that primary AML cells, but not normal CD34$^+$ cells, are at least partially dependent on SIRT5.

We engineered 22 AML cell lines to express doxycycline-sh*SIRT5*$^{2311/2312}$. In most cell lines, SIRT5 KD inhibited growth, reduced colony formation, and increased apoptosis, with the strongest effects on colony formation (Fig. 1D; Supplementary Fig. S2A–S2C). In seven lines (32%), colonies were reduced by >75%, in five lines (23%) by <25%, and by 25% to 75% in the remainder. The three lines most sensitive to *SIRT5* KD (CMK, SKM-1, OCI-AML2; referred to as SIRT5-dependent) and three lines most resistant to *SIRT5* KD (OCI-AML3, KG1a, Marimo; referred to as SIRT5-independent) were used in most subsequent studies (Fig. 1E and H). In view of the large range of sensitivity to *SIRT5* KD, we assessed potential correlations between SIRT5 dependence and genotype. However, next-generation sequencing of 52 genes recurrently mutated in myeloid malignancies in patient samples (Fig. 1A;

Figure 1. AML cells are selectively dependent on SIRT5. **A,** Primary AML samples ($N = 25$) were transduced with lentivirus for expression of RFP and doxycycline-inducible sh*SIRT5*^{2311} and sh*SIRT5*^{2312} (dox-sh*SIRT5*$^{2311/2312}$). RFP$^+$ cells were sorted and plated in colony assays ± doxycycline. Mutations in key AML genes are shown above. **B,** BM from *Sirt5*$^{+/+}$ and *Sirt5*$^{-/-}$ mice ($N = 3$ each) was transduced with plasmids containing AML oncogenes and plated in colony assays. Comparisons by multiple unpaired *t* tests. KO, knockout; WT, wild-type. **C,** Hematologic parameters were measured in 12-week-old *Sirt5*$^{+/+}$ and *Sirt5*$^{-/-}$ mice ($n = 5$ each). **D–H,** Twenty-two AML cell lines were engineered to stably express doxycycline-sh*SIRT5*$^{2311/2312}$, cultured ± doxycycline for 72 to 96 hours, and subjected to immunoblot and functional assays. **D,** Colony survival as a proportion of control. **E–H,** Analysis of representative SIRT5-dependent (OCI-AML2; CMK; SKM-1) and SIRT5-independent cell lines (KG1a, Marimo, and OCI-AML3). Dox, doxycycline. **E,** SIRT5 expression. **F,** Viable cells (MTS assay, unpaired *t* test). **G,** Colony survival (unpaired *t* test). **H,** Apoptosis (annexin V, multiple unpaired *t* tests). **I,** Viable cells (MTS assay, multiple unpaired *t* tests) in SKM-1 cells (SIRT5-dependent) and OCI-AML3 cells (SIRT5-independent) stably expressing three doxycycline-inducible shRNAs targeting different *SIRT5* sequences at 1 to 4 days after adding doxycycline. **J,** CRISPR/Cas9 was used to delete SIRT5 from CMK and OCI-AML3 cells. Single clones were selected and plated in colony assays ± doxycycline. Data represent the mean ± SEM from at least three independent experiments; comparisons by unpaired test. **K,** SKM-1 cells expressing doxycycline-sh*SIRT5*$^{2311/2312}$ were grown in regular (RM) or HS-5 conditioned medium (CM) ± doxycycline for 96 hours, and viable cells were quantified by ViaCount assay. Data were normalized to controls (no doxycycline; *, $P < 0.05$; **, $P < 0.01$; ***, $P < 0.001$).

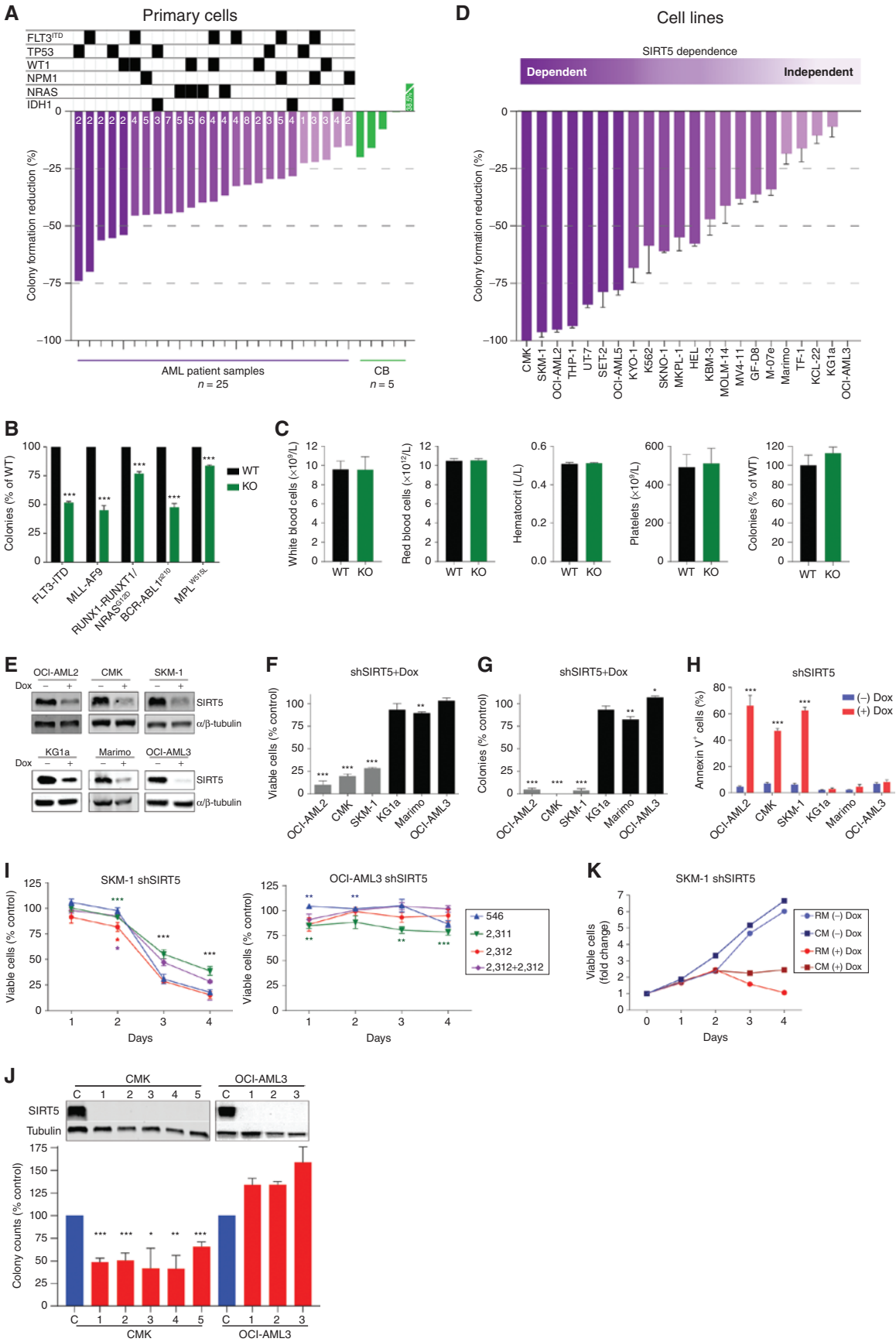
A
Primary cells
FLT3ITD
TP53
WT1
NPM1
NRAS
IDH1
Colony formation reduction (%)
AML patient samples n = 25
CB n = 5
D
Cell lines
SIRT5 dependence
Dependent
Independent
Colony formation reduction (%)
CMK
SKM-1
OCI-AML2
THP-1
U7-7
SET-2
OCI-AML5
KYO-1
K562
SKNO-1
MKPL-1
HEL
KBM-3
MOLM-14
MV4-11
GF-D8
M-07e
Marimo
TF-1
KCL-22
KG1a
OCI-AML3
B
Colonies (% of WT)
WT
KO
FLT3-ITD
MLL-AF9
RUNX1-RUNXT1/ NRASG12D
BCR-ABL1p210
MPL W515L
C
White blood cells (×10⁹/L)
Red blood cells (×10¹²/L)
Hematocrit (L/L)
Platelets (×10⁹/L)
Colonies (% of WT)
WT KO
E
OCI-AML2
CMK
SKM-1
KG1a
Marimo
OCI-AML3
Dox
SIRT5
α/β-tubulin
F
shSIRT5+Dox
Viable cells (% control)
G
shSIRT5+Dox
Colonies (% control)
H
shSIRT5
Annexin V+ cells (%)
(–) Dox
(+) Dox
I
SKM-1 shSIRT5
OCI-AML3 shSIRT5
Viable cells (% control)
Days
546
2,311
2,312
2,312+2,312
K
SKM-1 shSIRT5
Viable cells (fold change)
Days
RM (–) Dox
CM (–) Dox
RM (+) Dox
CM (+) Dox
J
CMK
OCI-AML3
SIRT5
Tubulin
Colony counts (% control)

Supplementary Table S1) and cell lines (Supplementary Table S4) failed to identify obvious correlations. Similarly, SIRT5 dependence was not correlated with SIRT5 protein expression (Supplementary Fig. S2D–S2F).

To rule out off-target shRNA effects, experiments were repeated with three doxycycline-inducible shRNAs and a non-inducible shRNA, each targeting different SIRT5 sequences, with consistent results (Fig. 1I; Supplementary Fig. S3A–S3C). Outgrowth after prolonged culture of SIRT5-dependent cells in doxycycline-containing media was associated with reexpression of SIRT5, suggesting cells are under selection pressure to reestablish SIRT5 expression (Supplementary Fig. S3D). Conditioned medium from HS-5 stromal cells can protect leukemia cells from cytotoxic and targeted therapies (47, 48), but did not protect AML cells from the effects of SIRT5 KD, consistent with the design of the initial screen (Fig. 1K; Supplementary Fig. S3E). Propidium iodide staining revealed increased sub-G_1 cells upon SIRT5 KD in SIRT5-dependent cell lines, indicating increased apoptosis, but the proportion of cells in G_0–1, S, and G_2–M phases remained stable. SIRT5 KD induced neither markers nor morphologic signs of differentiation. We also confirmed that doxycycline-sh*SIRT5*$^{2311/2312}$ had no significant effects on the expression of sirtuins other than SIRT5 (Supplementary Fig. S4A). Because doxycycline at high concentrations (~1 μg/mL) can inhibit mitochondrial protein synthesis (49, 50), we cultured parental cell lines in 100 ng/mL doxycycline, the concentration used in most experiments, but saw no effect (Supplementary Fig. S4B). Doxycycline at 6.25 ng/mL induced SIRT5 KD and growth inhibition in SIRT5-dependent cells as effectively as doxycycline at 100 ng/mL (Supplementary Fig. S4C and S4D). At yet lower concentrations, growth inhibition correlated with a decrease of SIRT5 protein, providing additional target validation (Supplementary Fig. S4E). Finally, we used CRISPR/Cas9 to generate single cell–derived *SIRT5*$^{-/-}$ cell lines. Compared with parental cells, *SIRT5* deletion significantly reduced colony formation by CMK cells (SIRT5-dependent), but not OCI-AML3 cells (SIRT5-independent; Fig. 1J).

SIRT5 Is Required for AML Establishment and Maintenance *In Vivo*

To test whether SIRT5 is required for AML establishment and maintenance *in vivo*, we injected NOD-SCID IL2Rγ$^{-/-}$ (NSG) mice with CMK (SIRT5-dependent) or OCI-AML3 cells (SIRT5-independent) coexpressing doxycycline-shSIRT5$^{2311/2312}$ and luciferase, and randomized at 18 hours after injection to doxycycline-containing or regular water (control). Mice injected with CMK cells maintained on doxycycline showed no luminescence at week 3 (Fig. 2A, left), while controls were strongly positive (Fig. 2A, right). We next randomized mice to continue their regimen or switch to doxycycline-containing or regular water, respectively. In mice started on doxycycline-containing water, irrespective of randomization, we observed no luminescence until termination of the experiment (week 13; Fig. 2A, left). There was no leukemic involvement on autopsy, and BM and spleen were negative for hCD45$^+$ (Fig. 2B, left and left middle panels). In the group started on regular water, mice switched to doxycycline-containing water at week 3 showed reduction of luminescence at week 4, cleared all luminescence at week 8, and survived until termination of the experiment, without evidence for leukemia at autopsy (Fig. 2B, right middle panel, and C). In contrast, mice continued on regular water died between weeks 4 and 5 with extensive leukemic involvement (Fig. 2A and B, right). Recipients of OCI-AML3 cells rapidly developed systemic disease (Fig. 2D), and died on day 31 (doxycycline) and 29 (control), with extensive leukemic involvement (Fig. 2E and F). SIRT5 KD was maintained in hCD45$^+$ cells from doxycycline-treated mice, confirming that *in vivo* survival of OCI-AML3 cells was not due to reexpression of SIRT5 (Fig. 2G).

To assess the role of SIRT5 in a syngeneic context, we infected BM from *Sirt5*$^{+/+}$ and *Sirt5*$^{-/-}$ mice with *MLL-AF9* retrovirus and injected 3×10^5 cells/mouse into lethally irradiated *Sirt5*$^{+/+}$ mice. In this aggressive AML model, median survival in recipients of *MLL-AF9*–transduced *Sirt5*$^{-/-}$ cells was 60 days versus 49 days for controls ($P = 0.428$; Fig. 3A), with similar GFP expression (86.4% ± 1.9% vs. 85.7±4.7%; $P = 0.9$). We transplanted 5×10^3 GFP$^+$Lin$^-$Kit$^+$ (LSK) cells/mouse from primary leukemic mice into secondary *Sirt5*$^{+/+}$ recipients. Recipients of *MLL-AF9*–transduced *Sirt5*$^{+/+}$ BM developed leukocytosis, with mostly GFP$^+$ cells, and showed massive splenomegaly at autopsy. White blood cells (WBC) in recipients of *Sirt5*$^{-/-}$ BM remained normal, with no or rare GFP$^+$ cells, and no splenomegaly in the majority (Fig. 3B and C). Median survival in recipients of *MLL-AF9/Sirt5*$^{+/+}$ cells was 23 days but had not been reached in recipients of *MLL-AF9/Sirt5*$^{-/-}$ cells at 8 weeks ($P < 0.0001$; Fig. 3C). Similarly, we infected BM cells from 5-fluorouracil (5-FU)–treated *Sirt5*$^{+/+}$ and *Sirt5*$^{-/-}$ mice with *BCR-ABL1*^{p210}-GFP retrovirus and injected 5,000 LSK cells/mouse into *Sirt5*$^{+/+}$ recipients. Median survival of mice receiving *Sirt5*$^{+/+}$ cells was 21 days, whereas 80% of mice receiving *Sirt5*$^{-/-}$ cells survived until day 47 (termination of experiment; $P < 0.01$; Fig. 3D). Finally, we probed the role of SIRT5 in a transgenic model of *FLT3-ITD*–positive myeloproliferative disease (MPD). The MPD in this model is mild, with modestly elevated WBCs and monocytosis at 4 to 6 months of age (51). *FLT3-ITD* transgenic mice were crossed with *Sirt5*$^{-/+}$ mice and bred to homozygosity, yielding

Figure 2. SIRT5 KD attenuates leukemia in a xenograft model. CMK cells (SIRT5-dependent) or OCI-AML3 cells (SIRT5-independent) expressing dox-sh*SIRT5*$^{2311/2312}$ and luciferase were engrafted into NSG mice. **A,** Mice engrafted with CMK cells ($N = 20$) were randomized between doxycycline-containing and regular water and followed by weekly bioluminescence imaging. At 3 weeks, groups were again randomized to continue their current regimen or switch to doxycycline-containing or regular water, respectively. Dox, doxycycline. **B,** At death or end of experiment, BM was analyzed by FACS for hCD45. A representative FACS plot was shown for each group. **C,** Kaplan–Meier analysis of survival of CMK-engrafted mice across all experimental conditions. **D,** Mice engrafted with OCI-AML3 ($N = 6$) cells were randomized between samples containing doxycycline and regular water and followed by weekly bioluminescence imaging. The luminescence scale is the same as in **A**. **E,** Kaplan–Meier analysis of survival for OCI-AML3–engrafted mice. **F,** BM was analyzed by FACS for hCD45. **G,** hCD45$^+$ spleen and BM cells from mice engrafted with OCI-AML3 cells were analyzed for SIRT5 expression by immunoblot (*, $P < 0.05$; **, $P < 0.01$; ***, $P < 0.001$).

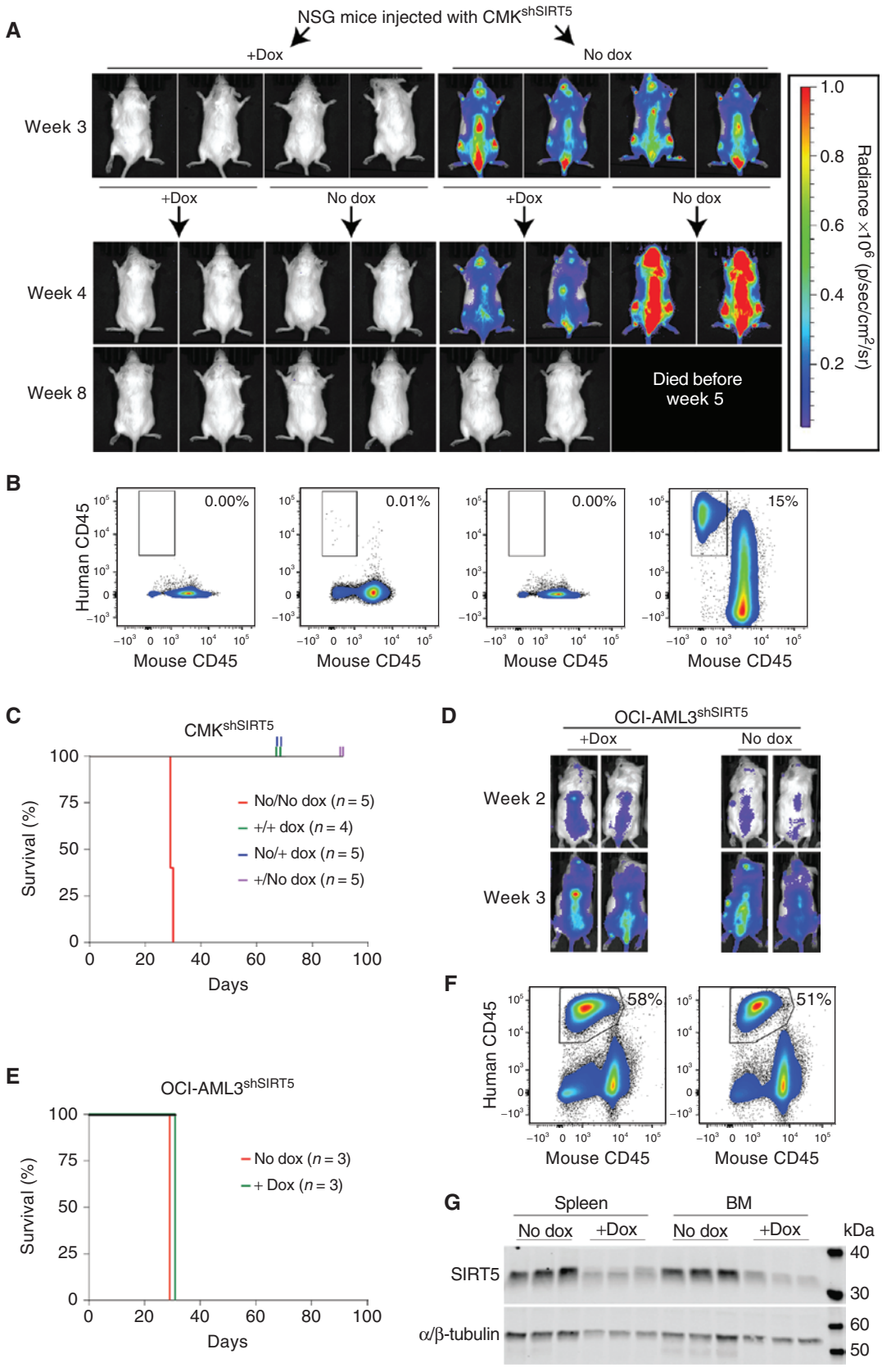
A
NSG mice injected with CMK^shSIRT5
+Dox
No dox
Week 3
Week 4
Week 8
Died before week 5
Radiance ×10^6 (p/sec/cm²/sr)
1.0
0.8
0.6
0.4
0.2
B
Human CD45
Mouse CD45
0.00%
0.01%
0.00%
15%
C
CMK^shSIRT5
Survival (%)
Days
No/No dox (n = 5)
+/+ dox (n = 4)
No/+ dox (n = 5)
+/No dox (n = 5)
D
OCI-AML3^shSIRT5
+Dox
No dox
Week 2
Week 3
E
OCI-AML3^shSIRT5
Survival (%)
Days
No dox (n = 3)
+ Dox (n = 3)
F
Human CD45
Mouse CD45
58%
51%
G
Spleen
BM
No dox
+Dox
kDa
SIRT5
α/β-tubulin
40
30
60
50

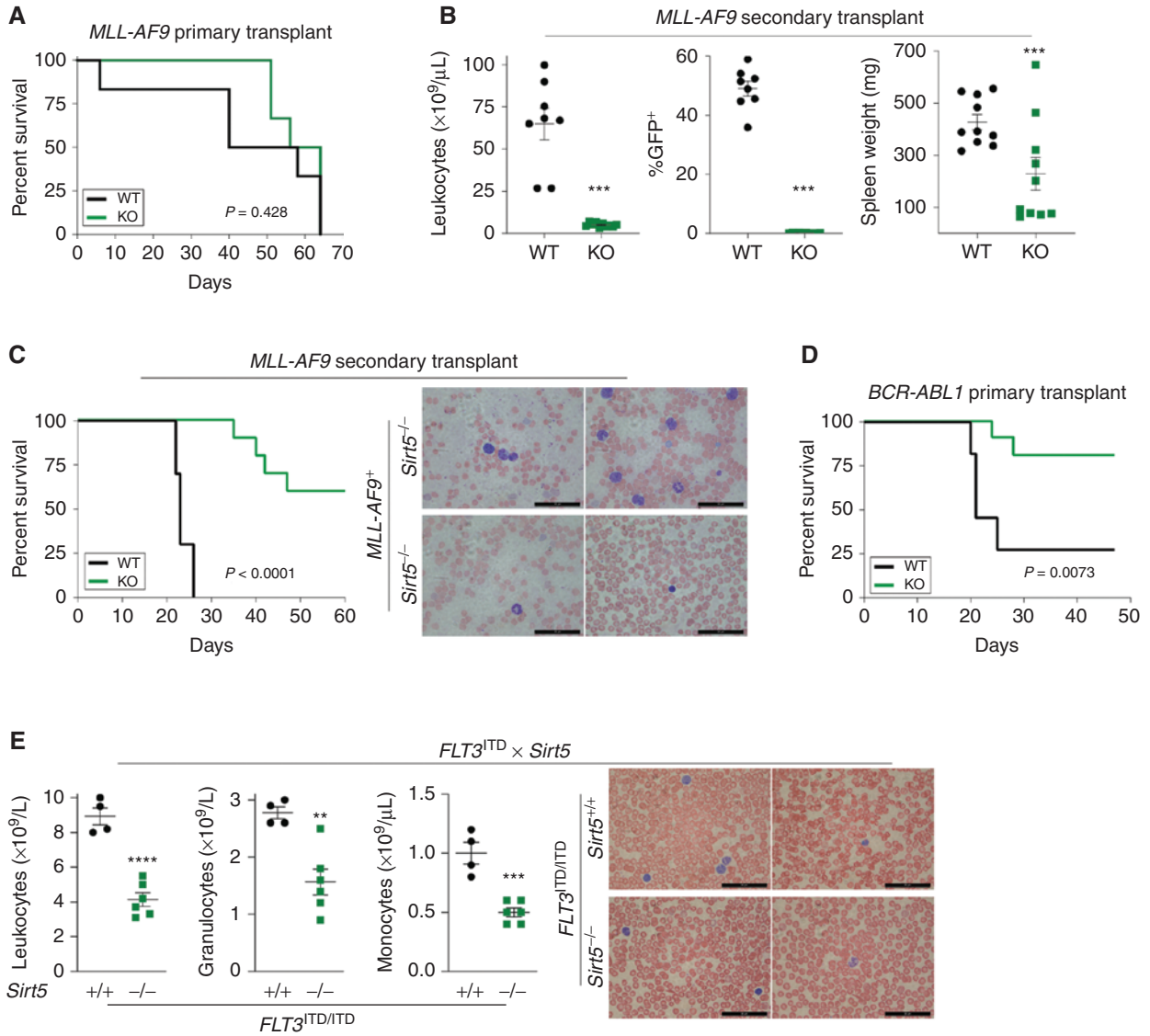

Figure 3. Absence of SIRT5 attenuates myeloid leukemia in syngeneic mouse models. **A,** BM from *Sirt5*$^{+/+}$ versus *Sirt5*$^{-/-}$ C57Bl6 mice was transduced with *MLL-AF9* retrovirus and injected into irradiated *Sirt5*$^{+/+}$ recipients. Kaplan–Meier survival analysis of primary recipients ($n = 6$/group). KO, knockout; WT, wild-type. **B,** GFP$^+$Lin$^-$Kit$^+$ BM cells were sorted from leukemic primary recipients and injected into secondary *Sirt5*$^{+/+}$ recipients. WBC counts and percent of GFP$^+$ blood cells were quantified at week 3, and spleen weights were measured at the time of sacrifice (unpaired *t* test). **C,** Left, Kaplan–Meier survival analysis of secondary recipients of *MLL-AF9*–expressing cells. Right, representative blood smears at week 3. **D,** Kaplan–Meier survival analysis of primary recipients of *BCR-ABL1*^{p210} transduced *Sirt5*$^{+/+}$ versus *Sirt5*$^{-/-}$ Lin$^-$Sca$^+$Kit$^+$ cells ($n = 10$/group). **E,** Left, WBC parameters in 5-month-old FLT3-ITD/*Sirt5*$^{+/+}$ (left; $n = 2$) compared with FLT3-ITD/*Sirt5*$^{-/-}$ mice ($n = 6$; right; unpaired *t* test). Right, representative blood smears at 5 months. The log-rank (Mantel–Cox) test was used for comparisons of survival (*, $P < 0.05$; **, $P < 0.01$; ***, $P < 0.001$). Scale bars in **C** and **E** are 50 micrometers.

FLT3$^{ITD/ITD}$/*Sirt5*$^{+/+}$ and *FLT3*$^{ITD/ITD}$/*Sirt5*$^{-/-}$ genotypes. At 5 months, WBCs, granulocytes, and monocytes were reduced in *FLT3*$^{ITD/ITD}$/*Sirt5*$^{-/-}$ compared with *FLT3*$^{ITD/ITD}$/*Sirt5*$^{+/+}$ mice (Fig. 3E). Altogether these data show that SIRT5 is required for leukemogenesis by several myeloid oncogenes.

SIRT5 Is Required for Oxidative Phosphorylation in SIRT5-Dependent AML Cells

SIRT5 desuccinylates multiple mitochondrial proteins, including electron chain components (34, 37, 38). To identify the mechanism by which SIRT5 KD kills SIRT5-dependent but not SIRT5-independent cells, we assessed mitochondrial protein succinylation in CMK cells (SIRT5-dependent) and KG1a cells (SIRT5-independent). Succinylation, malonylation, and acetylation increased in both upon SIRT5 KD, while glutarylation was low and unchanged, altogether suggesting that SIRT5 is active in SIRT5-dependent and SIRT5-independent cells (Fig. 4A; Supplementary Fig. S4F). AML cells depend on mitochondrial protein translation and OXPHOS, and exhibit reduced spare respiratory capacity (19, 25, 28). We measured the effect of SIRT5 KD on OXPHOS and glycolysis in AML cell lines upon SIRT5 KD. OXPHOS was consistently reduced in SIRT5-dependent cell lines, starting ~24 hours after doxycycline addition, but not in SIRT5-independent

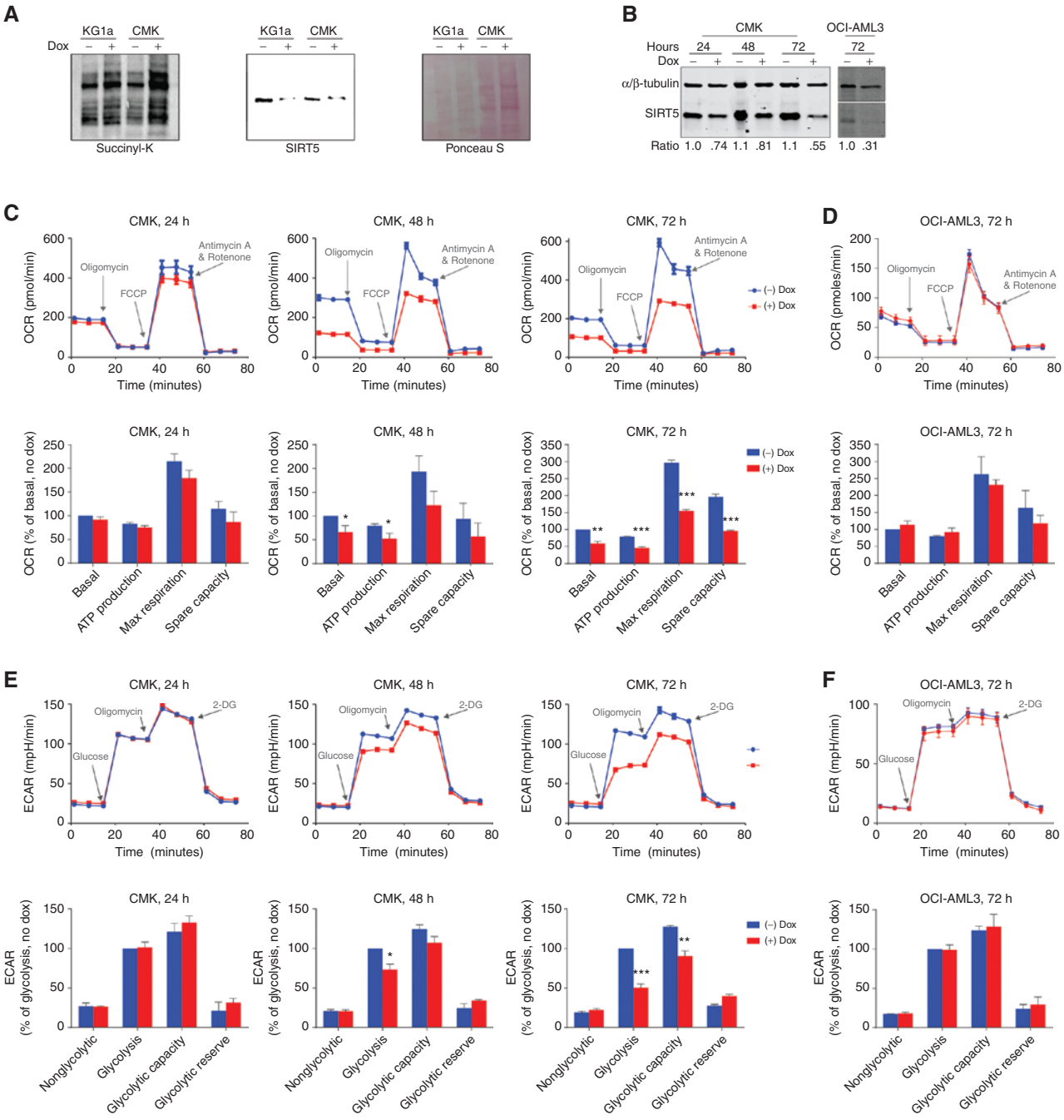

Figure 4. *SIRT5* KD reduces OXPHOS in SIRT5-dependent, but not SIRT5-independent, cell lines. **A,** CMK (SIRT5-dependent) and KG1a (SIRT5-independent) cells expressing doxycycline (dox)-sh*SIRT5*$^{2311/2312}$ were cultured ± 100 ng/mL doxycycline for 48 hours. Mitochondria were isolated and proteins resolved by SDS-PAGE, followed by immunoblotting with anti-succinyl-lysine and anti-SIRT5 antibodies, with Ponceau S staining as loading control. **B–F,** CMK (SIRT5-dependent) and OCI-AML3 (SIRT5-independent) cells expressing doxycycline-sh*SIRT5*$^{2311/2312}$ were cultured ± 100 ng/mL doxycycline for up to 72 hours and subjected to metabolic profiling. **B,** SIRT5 expression was assessed by immunoblot. **C,** Oxygen consumption rate (OCR) was measured in CMK cells on an Agilent Seahorse XFe96 Analyzer under basal conditions and under stress (for details, see Methods). Top, Representative experiment. Bottom, Means of three independent experiments. **D,** OCI-AML3 cells were cultured ± doxycycline for 72 hours and OCR was measured as in **B**. Top, Representative experiment. Bottom, means of three independent experiments. **E,** ECAR as a proxy for glycolysis was measured upon SIRT5 KD in CMK cells under basal conditions and stress. Top, Representative experiment. Bottom, Means of three independent experiments. **F,** OCI-AML3 cells expressing doxycycline-sh*SIRT5*$^{2311/2312}$ were cultured ± doxycycline for 72 hours, and ECAR was measured as in **D**. Data represent the mean ± SEM from three independent experiments. Comparisons were performed with multiple unpaired *t* tests (*, $P < 0.05$; **, $P < 0.01$; ***, $P < 0.001$).

lines (Fig. 4B–D; Supplementary Fig. S5A and S5B). Extracellular acidification rate (ECAR) as a measure of glycolysis was also reduced only in SIRT5-dependent cells, but changes tended to occur later (Fig. 4E and F; Supplementary Fig. S5C). As previous work has shown that SIRT5 KD induces mitophagy in breast cancer cells (52), we analyzed mitochondrial morphology but saw no obvious differences between SIRT5-dependent and –independent cell lines with or without SIRT5 KD (Supplementary Fig. S5D), and mitochondrial DNA copy numbers as assessed by qPCR for the mitochondrially encoded NADH:ubiquinone oxidoreductase core subunit 1 (ND1) were similar (Supplementary Fig. S5E). Chronic ethidium bromide exposure depletes mitochondrial DNA, allowing us to test whether OXPHOS is essential for viability (53). Derivative cell lines devoid of mitochondrial DNA are referred to as ρ_0 cells. Repeated attempts to generate ρ_0 derivatives from SIRT5-dependent lines failed (Supplementary Fig. S5F), while ρ_0 cells were readily established from SIRT5-independent lines. KD of SIRT5 in these ρ_0 lines had minimal effects on growth and viability, suggesting that independence of SIRT5 and OXPHOS cosegregate (Supplementary Fig. S5G and S5H).

SIRT5 KD Induces Oxidative Stress in SIRT5-Dependent, but Not SIRT5-Independent, AML Cells

We next assessed the activation state of canonical signaling pathways, including stress-activated protein kinase, MAPK, S6 kinase, PI3K, STAT5, SHP2, and SRC, but found no evidence for SIRT5-dependent regulation (Supplementary Fig. S6A). AML cells with low spare respiratory capacity are susceptible to oxidative stress (19). To test whether cell death induced by SIRT5 KD is caused by increased oxidative stress, we measured mitochondrial superoxide by flow cytometry. SIRT5 KD increased superoxide in SIRT5-dependent cells, but not in SIRT5-independent cells (Fig. 5A–D). The superoxide increase preceded apoptosis and was partially rescued by vitamin E, but not other antioxidants (Fig. 5B and C; Supplementary Fig. S6B). Superoxide dismutase 2 (SOD2) detoxifies mitochondrial superoxide to oxygen and hydrogen peroxide, which is converted to oxygen and water by catalase. We compared SOD2 expression in SIRT5-dependent and SIRT5-independent AML cells but found no differences (Supplementary Fig. S6C). However, ectopic SOD2 expression blunted the superoxide increase induced by SIRT5 KD in CMK cells, reduced apoptosis, and partially restored colony formation (Fig. 5E and F). Strikingly, SOD2 KD induced growth inhibition and apoptosis only in SIRT5-dependent cell lines (Fig. 5G and H). In contrast, ectopic expression of SOD1 failed to rescue SIRT5-dependent cell lines from the effects of SIRT5 KD (Supplementary Fig. S6D). In addition, measurement of SOD2 activity revealed no change after KD of SIRT5, suggesting that SOD2 is not a direct target of SIRT5 (Supplementary Fig. S6E). We next measured the NAD^+/NADH ratio and GSH level as a measure of redox buffer capacity. Both NAD^+/NADH and GSH decreased upon SIRT5 KD in SIRT5-dependent but not SIRT5-independent cell lines (Fig. 5I), suggesting that SIRT5-dependent AML cell lines require SIRT5 to reduce mitochondrial superoxide and maintain redox homeostasis to prevent apoptosis.

SIRT5 Regulates Glutamine Metabolism in SIRT5-Dependent AML Cells

To identify SIRT5-regulated metabolic pathways in AML cells, we performed untargeted metabolomics on SIRT5-dependent (CMK and SKM-1) and SIRT5-independent (OCI-AML and KG1a) cell lines expressing doxycycline-sh*SIRT5*$^{2311/2312}$ at 36 and 48 hours after the addition of doxycycline. Steady-state levels of multiple metabolites were altered upon SIRT5 KD, often in opposite directions according to SIRT5 dependency (Supplementary Fig. S7A and S7B). Profound reductions in tricarboxylic acid (TCA) cycle intermediates and amino acids were observed in SIRT5-dependent lines, while their concentrations were increased in SIRT5-independent cell lines. We used Ingenuity Pathway Analysis (IPA) to identify metabolic networks altered by SIRT5 KD and attribute metabolite alterations to pathways. We observed mostly consistent changes in TCA cycle metabolites, which were linked to SIRT5 (Supplementary Fig. S7C). IPA also identified potential upstream regulators, including GLS and α-ketoglutarate (Supplementary Fig. S7D). At a global level, the pathways implicated by IPA were remarkably consistent, yet mostly regulated in opposite directions, in accord with the changes in total metabolite concentrations. Top IPA hits included RNA charging as well as alanine and serine metabolism (Supplementary Fig. S8).

GLS converts glutamine to glutamate, which is metabolized to α-ketoglutarate by glutamate dehydrogenase 1 (GLUD1) or aminotransaminases (GOT1/2, GPT2, and PSAT1). Recent studies have shown that SIRT5 promotes breast cancer by activating GLS and colorectal cancer by activating GLUD1 (54, 55). As previous work has shown that some AML cells are glutamine dependent and suggested a role for GLS in constraining *de novo* glutathione synthesis in AML, we hypothesized that SIRT5-dependent AML cell lines may require SIRT5 for regulating glutamine metabolism (24, 27, 56). To test this, we performed stable isotope metabolic tracing experiments using [$^{13}C_5$,$^{15}N_2$]-glutamine or [1,2,3–$^{13}C_3$]-glucose in SIRT5-dependent and SIRT5-independent cells (Fig. 6A; Supplementary Fig. S9A). To ensure the metabolite changes are due to SIRT5 KD, but not cell death, cells were analyzed after 36 hours in doxycycline, when cell viability was >90%. Initial time course experiments were performed in SKM-1 cells. [1,2,3–$^{13}C_3$]-glucose tracing did not show significant changes in glycolytic flux upon SIRT5 KD, consistent with Seahorse experiments showing reduced ECAR only at relatively late time points (Fig. 4E; Supplementary Fig. S5B). The glutamine/glutamate ratio was markedly increased in SIRT5-dependent cells and further elevated upon SIRT5 KD (Fig. 6B). Glutamine abundance was much higher in SIRT5-dependent cells at baseline and altered by SIRT5 KD only in SIRT5-dependent cell lines. In addition, only SIRT5-dependent cell lines showed altered abundances of TCA cycle intermediates upon SIRT5 KD (Fig. 6C; Supplementary Fig. S9B). In light of the results above, we hypothesized that SIRT5-dependent AML requires SIRT5 to regulate glutamine flux to sustain redox homeostasis and/or anabolism. To test this, we cultured SIRT5-dependent and SIRT5-independent cells with or without glutamine, and measured apoptosis. SIRT5-dependent cell lines were more sensitive to glutamine deprivation than SIRT5-independent cell lines (Fig. 6D). Moreover, glutamine withdrawal and SIRT5 KD were synergistic (Fig. 6E).

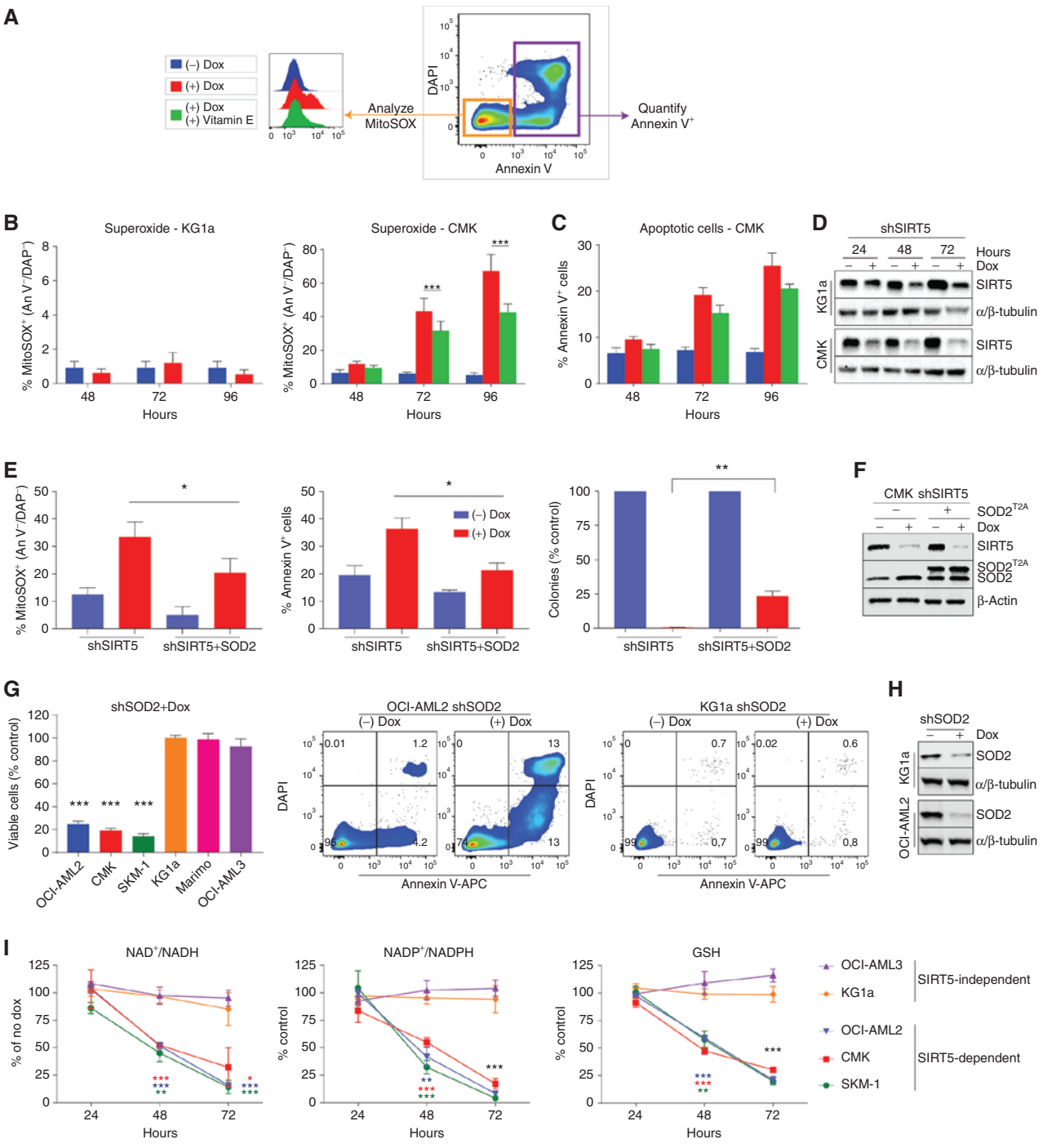

Figure 5. *SIRT5* KD induces mitochondrial superoxide in SIRT5-dependent, but not SIRT5-independent, cell lines. **A–D,** KG1a cells (SIRT5-independent) and CMK cells (SIRT5-dependent) expressing doxycycline (dox)-sh*SIRT5*$^{2311/2312}$ were cultured for 96 hours ± 100 ng/mL doxycycline ± vitamin E (200 μmol/L). Following culture, cells were analyzed by FACS after staining with MitoSOX dye to measure mitochondrial superoxide, annexin V (An V) to identify apoptotic cells, and DAPI (DAP) to identify dead cells. Data represent three independent experiments. **A,** Gating strategy. **B,** Percent of KG1a and CMK cells positive for mitochondrial superoxide but negative for annexin V (multiple unpaired *t* tests). **C,** Percent CMK cells positive for annexin V. **D,** SIRT5 expression (immunoblot). **E** and **F,** CMK cells expressing doxycycline-sh*SIRT5*$^{2311/2312}$ engineered to ectopically express SOD2 were cultured ± doxycycline for 72 hours. **E,** Left, percent MitoSOX$^+$/annexin V$^-$/DAPI$^-$ cells. Middle, percent annexin V$^+$ cells. Right, colony formation. Comparisons were performed with paired *t* test. **F,** SOD2 expression (immunoblot). **G,** SIRT5-independent (KG1a; Marimo; OCI-AML3) and SIRT5-dependent (CMK; OCI-AML2, SKM-1) cell lines expressing doxycycline-inducible sh*SOD2* were cultured in 100 ng/mL doxycycline. Left, viable cells (MTS assay) after 96 hours. Comparisons were performed with multiple paired *t* test. Middle, apoptosis (annexin V staining) in OCI-AML2 cells. Right, apoptosis (annexin V staining) in KG1a cells. **H,** Immunoblot analysis of SOD2 expression shown for KG1a and OCI-AML2 cells. **I,** NAD$^+$/NADH ratio was measured by GLO assay in SIRT5-independent (OCI-AML3; KG1a) and SIRT5-dependent (OCI-AML2; CMK; SKM-1) cell lines expressing doxycycline-sh*SIRT5*$^{2311/2312}$ at 24 to 72 hours after addition of 100 ng/mL doxycycline. Data represent the mean ± SEM from three independent experiments. Comparisons were performed with multiple unpaired *t* tests (*, $P < 0.05$; **, $P < 0.01$; ***, $P < 0.001$).

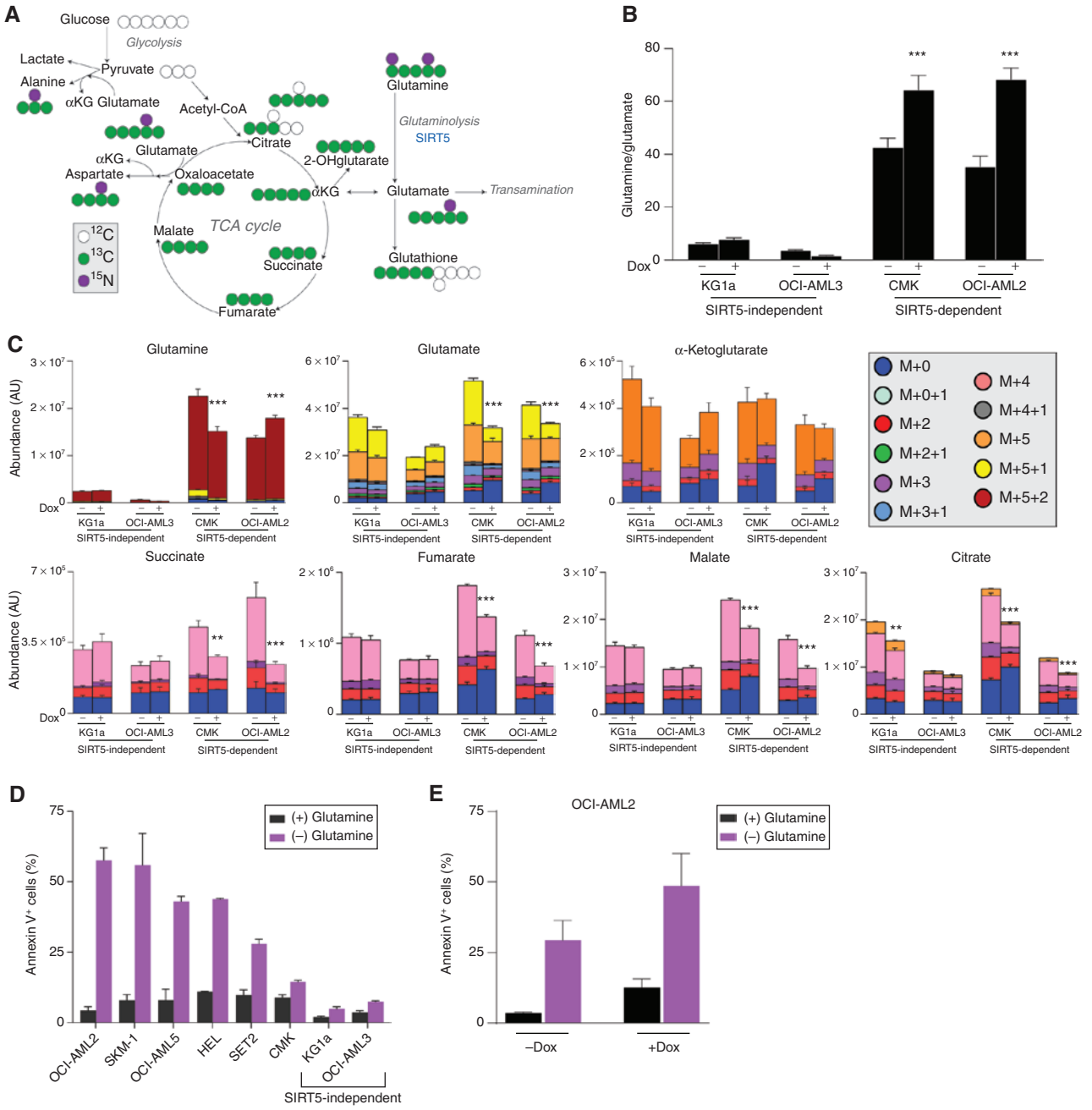

Figure 6. SIRT5 regulates glutamine metabolism in SIRT5-dependent AML cells. **A,** Overview of the predicted isotopologues for metabolites downstream to [$^{13}C_5$,$^{15}N_2$]-glutamine in tracing experiments. αKG, α-ketoglutarate. **B,** Ratio of isotope-labeled glutamate/glutamine, with comparisons by two-way ANOVA and Tukey correction for multiple comparisons. Dox, doxycycline. **C,** Four-hour glutamine tracing results for two SIRT5–independent (KG1a, OCI-AML3) and -dependent (CMK, OCI-AML2) AML cell lines, with comparisons by two-way ANOVA and Tukey correction for multiple comparisons. **D,** Apoptosis in SIRT5-dependent and -independent cell lines cultured ± l-glutamine for 72 hours. **E,** Apoptosis in OCI-AML2 shSIRT5 cells cultured ± doxycycline ± glutamine for 48 hours. Data represent the mean ± SEM from at least three independent experiments (*, $P < 0.05$; **, $P < 0.01$; ***, $P < 0.001$).

A Small-Molecule SIRT5 Inhibitor Selectively Inhibits Cell Proliferation, Metabolism, and Colony Formation of AML Cells

To assess the potential of targeting SIRT5 catalytic activity in AML, we tested several published SIRT5 inhibitors in cell proliferation assays of AML cells and normal controls but found them indiscriminately toxic or inactive (52, 57). To overcome this limitation, we synthesized a prodrug of SIRT5 inhibitor 1 (S5I1) named ethyl 3-(3-((S)-6-(((S)-1-(cyclobutylamino)-3-(1H-indol-3-yl)-1-oxopropan-2-yl)amino)-5-((3-fluorophenyl) sulfonamido)-6-oxohexyl)thioureido)propanoate (NRE139; Fig. 7A; Supplementary Fig. S10). The parent inhibitor, S5I1, inhibits SIRT5 with an IC_{50} of 110 nmol/L in a published

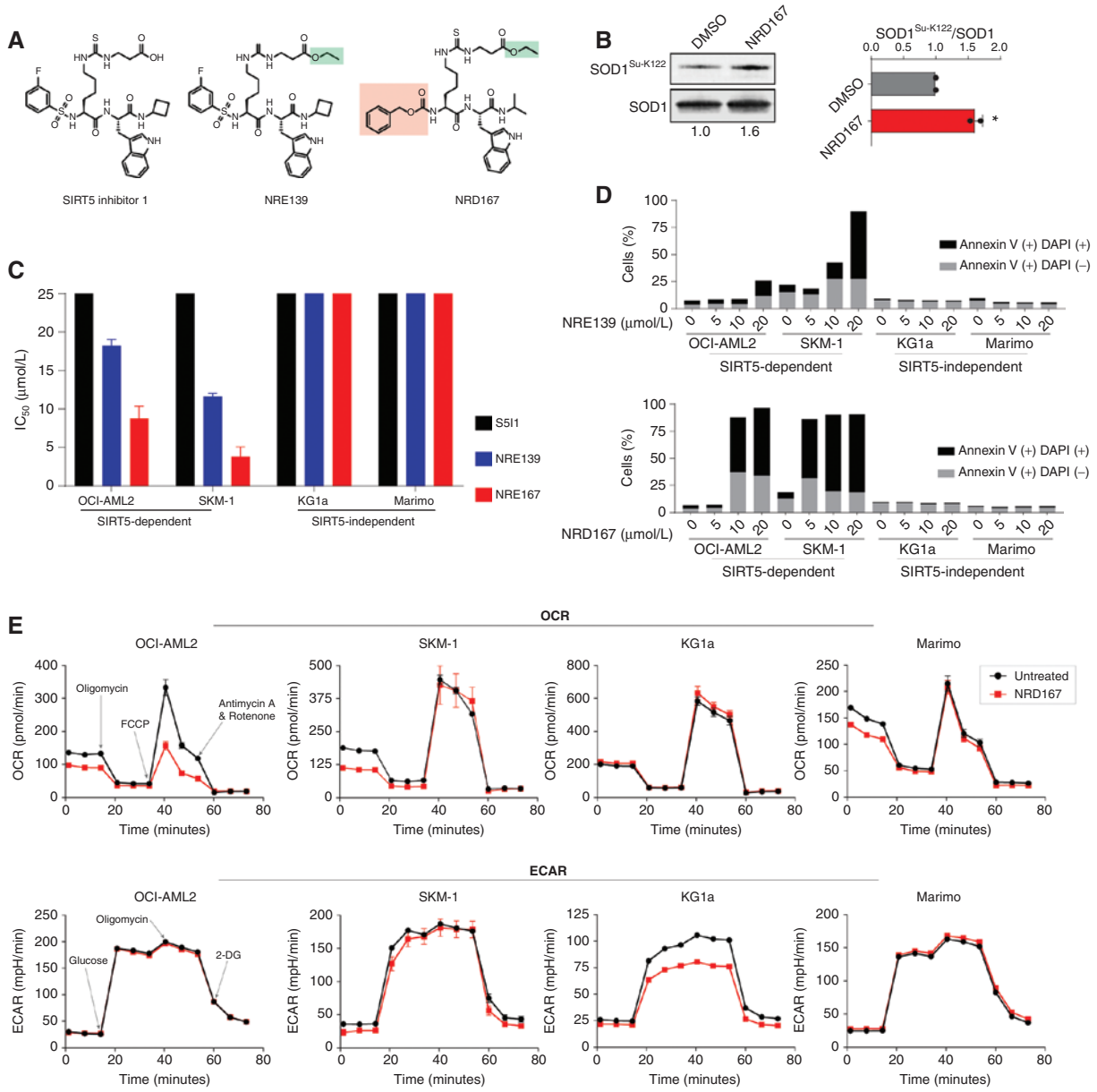

Figure 7. A small-molecule SIRT5 inhibitor, NRD167, recapitulates SIRT5 KD effects on AML cells. **A,** Structures of SIRT5 inhibitor 1, NRE139, and NRD167. **B,** HEK cells expressing FLAG-SOD1 were treated with NRD167 for 18 hours. SOD1 immunoprecipitates were probed with anti–succinyl-lysine 122 serum. One representative experiment is shown. **C** and **D,** Two SIRT5-dependent (OCI-AML2; SKM-1) and two SIRT5-independent (KG1a; Marimo) cell lines were treated with graded concentrations of SIRT5 inhibitor 1, NRE139, and NRD167 for 72 hours. **C,** Viable cells were quantified by MTS assay, and IC_{50} values were calculated **D,** Apoptosis was quantified by FACS for annexin V and DAPI. **E,** Cells were treated with NRD167 for 24 hours, and OCR and ECAR were determined by Seahorse. (*continued on next page*)

biochemical assay (58) but exhibits no activity in cell-based assays. Presumably, S5I1 does not enter cells, partly due to a negatively charged carboxylate moiety. We modified S5I1 by masking the carboxylate as the corresponding ethyl ester NRE139, enabling cellular uptake. Inside the cell, NRE139 is converted into S5I1 by ubiquitous esterases. In addition, we included the structurally closely related prodrug NRD167 (Fig. 7A). To confirm that NRD167 is cell permeant and inhibits SIRT5 catalytic activity, HEK293 cells expressing FLAG-tagged SOD1 were treated with vehicle or NRD167 (10 μmol/L) for 18 hours. FLAG-tagged SOD1 was immunoprecipitated, followed by immunoblotting with an antibody raised against SOD1 succinyl-lysine 122, a documented SIRT5 target (59, 60). Succinylation of SOD1 at lysine 122 was increased in the presence of NRD167 (Fig. 7B). The effect of S5I1, NRE139, and NRD167 was compared against SIRT5-dependent (OCI-AML2 and SKM-1) and SIRT5-independent cell lines (KG1a and Marimo). As expected, S5I1 was inactive. NRE139 and NRD167 selectively inhibited cell proliferation and induced apoptosis in SIRT5-dependent cells, with minimal effects on SIRT5-independent cells. NRD167 was more

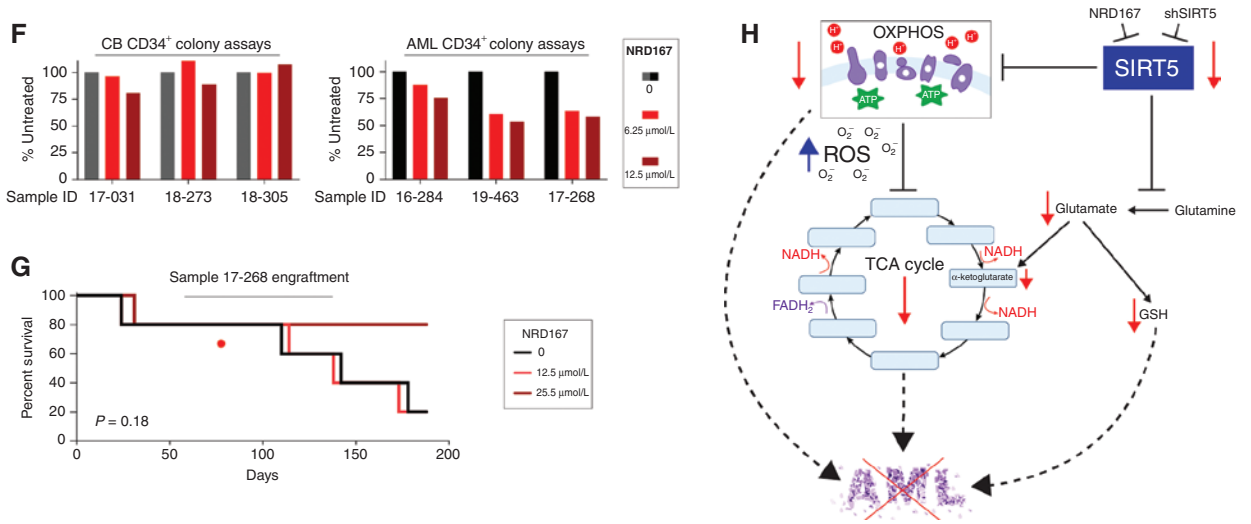

Figure 7. ***(Continued)*** **F,** CD34+ cells purified from three primary AML and three CB samples were cultured in colony assays ± NRD167 for 12 to 14 days. **G,** Survival of NSG-SGM3 mice injected with cells from AML sample 17-268 treated *in vitro* with NRD167 for 72 hours. **H,** Schematic depicting metabolic consequences of SIRT5 KD in AML cells. ROS, reactive oxygen species.

potent than NRE139, inhibiting proliferation of SIRT5-dependent cell lines with an IC_{50} of 5 to 8 μmol/L and inducing >80% apoptosis at 5 to 10 μmol/L (Fig. 7C and D), and was chosen for further evaluation. Globally NRD167's effects on OXPHOS and ECAR, as assessed by Seahorse, resembled those of SIRT5 KD (Fig. 7E), suggesting that inhibition of SIRT5 catalytic activity is sufficient to reproduce the metabolic consequences of SIRT5 KD, although subtle differences were noted such as a decrease in ECAR with NRD167 in KG1a cells and preserved spare oxidative capacity in SKM-1 cells. Next, NRD167 was tested against CD34+ cells from patients with AML and CB CD34+ cells in colony assays ($n = 3$ each; Fig. 7F). Reduction of colony formation was significantly more pronounced in AML versus CB samples (6.25 μmol/L: 70% ± 8.6% vs. 102% ± 4.4%, $P = 0.03$; 12.5 μmol/L: 62% ± 6.7% vs. 92% ± 7.9%, $P = 0.044$). Cells from sample 17-268 were treated *ex vivo* with NRD167 for 72 hours and then injected into NSG-SGM3 mice. The survival of mice injected with NRD167-treated cells trended longer compared with controls (Fig. 7G). These data implicate SIRT5 catalytic activity as a potential therapeutic target in AML.

DISCUSSION

We discovered that SIRT5 KD reduced colony formation by >25% to 100% in 80% of primary AML samples and 77% of AML cell lines, while colony formation by normal CD34+ cells was unaffected. Genetic absence of SIRT5 impairs transformation of primary hematopoietic cells by AML-associated oncogenes *in vitro*, and absence of SIRT5 attenuates myeloid leukemia *in vivo*. Similar to BCL2, SIRT5 dependence is not associated with particular genotypes, and extends to p53- and N/KRAS-mutated cells, suggesting that targeting SIRT5 may be effective in these challenging cases.

Through a combination of steady-state measurements and metabolic tracing with stable isotope–labeled substrates, we identified a role for SIRT5 in regulating glutaminolysis in multiple SIRT5-dependent cell lines. Decreased glutaminolysis upon SIRT5 KD in SIRT5-dependent, but not -independent cells, was accompanied by an increase in mitochondrial superoxide that preceded apoptosis, and was partially rescued by vitamin E or ectopic SOD2. Consistent with a critical role for this pathway, SIRT5-dependent AML cell lines were highly sensitive to SOD2 KD. In striatonigral neurons of *Sirt5*$^{-/-}$ mice challenged with the reactive oxygen species (ROS) inducer MTPT, SOD2 expression decreases much more than in *Sirt5*$^{+/+}$ controls, although the mechanism for this is unknown (42). In contrast, SIRT5 KD had no effect on SOD2 expression in AML cells. While SIRT3 has been shown to positively regulate SOD2 by lysine deacetylation (61), there is no evidence that deacylation of any SOD2 lysines is controlled by SIRT5 (34, 35, 37, 38). Consistent with this, SOD2 activity was unaffected by SIRT5 KD in OCI-AML2 cells, suggesting that the increase in superoxide is caused by an alternative mechanism. Regardless, our data implicate glutamine metabolism in maintaining redox homeostasis in AML cells, adding to previous evidence pointing to glutamine as an AML vulnerability (23, 24, 26, 27, 56). We have now identified SIRT5 as a master regulator of this process in AML.

SIRT5 may regulate glutamine metabolism at several levels and in a cell type–specific manner. In colorectal cancer, SIRT5 was shown to activate GLUD1 through deglutarylation, thereby increasing α-ketoglutarate concentrations (54). In contrast, SIRT5-dependent desuccinylation of GLS K164 in breast cancer protects GLS from ubiquitination at K158 and subsequent degradation (55). Similar to the latter study, we find that SIRT5 KD increases the glutamine/glutamate ratio in SIRT5-dependent, but not SIRT5-independent, AML cell lines, consistent with positive regulation of GLS by SIRT5. Strikingly, [$^{13}C_5{}^{15}N_2$]-glutamine at steady state is much higher in SIRT5-dependent compared with SIRT5-independent cell lines, suggesting fundamental differences in glutamine uptake. However, RNA sequencing shows comparable expression of the main glutamine transporter SLC1A5, and additional studies are needed to clarify the underlying

mechanism. Consistent with a potential role of SIRT5 in promoting entrance of glutamate-derived carbon atoms into the TCA cycle, we find that SIRT5 KD reduces the steady-state levels and [$^{13}C_5{}^{15}N_2$]-glutamine–derived labeled isotopologues of TCA cycle metabolites in multiple SIRT5-dependent cell lines. This may explain the reduction of OXPHOS and spare oxidative reserve capacity in response to SIRT5 KD, a consistent finding in Seahorse experiments on SIRT5-dependent cell lines. This feature appears to be at least in part constrained by decreased flux through α-ketoglutarate dehydrogenase (which binds to and feeds complex I; ref. 62) downstream of glutaminolysis. Alternatively, by regulating glutathione synthesis via glutaminolysis, SIRT5 may participate in glutathionylation of succinate dehydrogenase (SDH; complex II), which was previously associated with increases in OXPHOS in leukemia stem cells from patients with AML (63). It remains possible that SIRT5 directly regulates OXPHOS, corresponding to the presence of SIRT5-regulated lysines in respiratory chain complex proteins (34, 37). In complex V, 12 lysine succinylation sites are identified, including K97 with >300-fold increased stoichiometry in *Sirt5*$^{-/-}$ liver mitochondria (37). SIRT5 enhances OXPHOS in HEK293T cells and *Sirt5*$^{-/-}$ murine embryonic fibroblasts (MEF) exhibit reduced OXPHOS and spare reserve capacity (64, 65). In contrast, Park and colleagues report that SIRT5 inhibits SDH (complex II) in MEFs through desuccinylation of lysines in the SDHA/B subunits (34). Our data implicate SIRT5 as a positive regulator of OXPHOS in SIRT5-dependent AML cells, although precisely elucidating the mechanism will require additional studies. The fact that OXPHOS is regulated by SIRT5 in SIRT5-dependent, but not SIRT5-independent, AML cells lines aligns well with our inability to generate ρ_0 derivatives from SIRT5-dependent cell lines. Mitochondria from some AML cases are increased in size, but reduced in number, and have lower activity of mitochondrially encoded respiratory chain complexes III, IV, and V; while mitochondrial mass is increased, spare reserve capacity is reduced, and cells are dependent on OXPHOS (19). These features are also exhibited by AML leukemia-initiating cells, which, unlike hematopoietic stem cells, use OXPHOS as their main energy source, with limited glycolysis capacity in anaerobic conditions (13, 28). In line with this, knockout of genes driving mitochondrial processes, including OXPHOS, sensitizes AML cells to venetoclax (14, 15).

In aggregate, our data indicate that SIRT5 is critical for metabolic adaptability in a large subset of primary AML cases and cell lines, similar to its role in healthy tissues under stress (42, 43, 45, 66). Because SIRT5 regulates several important metabolic pathways (Fig. 7G), it is conceivable that inhibiting SIRT5 would avoid the rapid adaptation that limits the efficacy of targeting single metabolic pathways in cancer. From a clinical perspective, it would be important to identify a biomarker of SIRT5 dependence, but we found no obvious correlation between SIRT5 dependence and AML genotype or SIRT5 expression. Similarly, correlations between BCL2 expression or specific somatic mutations and AML responses to venetoclax are weak (67, 68). The effects of venetoclax on AML stem cells are mediated through the inhibition of OXPHOS (13, 69), indicating that metabolic vulnerabilities in AML can be genotype agnostic and involve critical regulators that are neither mutated nor aberrantly expressed. The sensitivity to SIRT5 disruption may therefore reflect a specific metabolic phenotype generated by multiple alternative mechanisms that turn SIRT5 into a bottleneck, similar to SIRT3's role in diffuse large B-cell lymphoma (70). For instance, reactive acyl-CoA species may create "carbon stress" due to nonenzymatic protein lysine acylation and cells with high steady-state concentrations of acyl-CoA species may be particularly dependent on SIRT5 for the maintenance of proper protein function (71). Ongoing work in our lab is seeking to identify metabolic markers of SIRT5 dependence.

Although the SIRT5 catalytic pocket exhibits several unique features, published compounds either lack potency or selectivity over other sirtuins, or are peptide based with insufficient cell permeability (39). To the best of our knowledge, no clinical SIRT5 inhibitors have been reported to date. We have identified NRD167 as a potent, cell-permeant SIRT5 inhibitor that overcomes several of the limitations of previous SIRT5 inhibitors. While NRD167's limited bioavailability precludes *in vivo* studies, inhibition of SIRT5 catalytic activity with NRD167 mirrors the phenotypic consequences of SIRT5 KD, selectively inhibiting AML over CB CD34$^+$ cells and SIRT5-dependent over SIRT5-independent AML cell lines. These data provide a strong rationale for the development of clinical SIRT5 inhibitors to treat AML.

METHODS

Patient Samples

This study was approved by the University of Utah Institutional Review Board, based on the recommendations of the Belmont Report, and all patients provided written informed consent to protocol 45880 before donating samples. Mononuclear cells (MNC) or CD34$^+$ cells were isolated from blood or BM of patients with newly diagnosed (N = 48), relapsed/refractory AML (N = 5), and one unknown using Ficoll-Paque Premium (GE Healthcare) and an AutoMACS Pro Separator (Miltenyi Biotec). Twelve samples (unique patients) were used in the initial shRNA screen and 51 in subsequent experiments. For clinical and molecular diagnostic details, see Supplementary Table S1.

shRNA Library Screen

Lentiviral shRNA Library. A custom pooled shRNA library targeting leukemia-related genes was provided by Cellecta (http://www.cellecta.com). This library contains 10,091 shRNAs targeting 1,287 genes associated with leukemia, as well as positive and negative control shRNAs (Supplementary Table S5). The shRNA constructs were designed in a pRSI16 Clonal Barcode vector containing a puromycin-resistant gene (Puro^R) and a red fluorescent protein (RFP) marker (TagRFP). Each shRNA was linked to a unique 8-bp barcode identifiable by sequencing. The pooled shRNA library was received as packed lentiviral particles. The titer of the leukemia library stocks was determined by the manufacturer as 1.56×10^9 TU/mL.

Infection of Primary AML Cells. MNCs were cultured at up to 5×10^6 cells/mL in RPMI supplemented with 10% FBS (Sigma-Aldrich), 2 mmol/L L-glutamine, 100 U/mL penicillin/streptomycin plus CC100 (StemCell Technologies), GM-CSF (10 ng/mL), and G-CSF (10 ng/mL; PeproTech). At 48 hours, cells were diluted to 10^6/mL and distributed into 6-well plates at 2 mL/well. shRNA lentiviral particles were added, targeting a multiplicity of infection (MOI) of 0.3, followed by the addition of polybrene (2 μg/mL) and HEPES buffer (Invitrogen; 10 mmol/L). The cells were centrifuged at 1,800 rpm for 90 minutes at 32°C. Following centrifugation, the plates were kept in a humidified incubator at 5% CO_2 and 37°C. The medium was

replaced with fresh medium at 12 to 18 hours after transduction. At 72 hours after transduction, the cells were pooled and RFP$^+$ cells quantified by flow cytometry [Becton-Dickinson (BD) FACSAria II].

Culture and Selection. At 48 hours after the infection of the AML cells, HS-5 human stromal cells (a kind gift of Dr. Beverly Torok-Storb, University of Washington, Seattle, WA; ref. 46) were plated in 6-well plates at 3×10^5 cells/well and cultured for 24 hours in RPMI1640 medium supplemented with 10% FBS. At this point, the infected AML cells were layered on top of the adherent HS-5 cells, without additional cytokines. The medium was changed every 24 hours. To avoid depleting the cytokines produced by HS-5 cells, half of the medium was removed from each well and pooled. The AML cells were spun down, and the supernatant was removed. Next, the cells were resuspended in fresh medium, and an equal volume of the previously pooled medium was redistributed to each well. After 7 to 9 days of coculture, the AML cells growing in suspension were removed and pooled. To quantitatively collect all AML cells attached to HS-5 cells, the cells were trypsinized and sorted for RFP$^+$ on a BD FACSAria II. The sorted RFP$^+$ cells were combined with the remaining AML cells, pelleted, and stored for subsequent DNA extraction.

DNA Extraction and Sequencing of Barcodes. The cell pellets were resuspended in Qiagen Buffer P1 supplemented with 100 μg/mL RNase A (Qiagen) at a concentration of 10^7 cells/mL and mixed with 1/20 volume of 10% SDS followed by incubation for 5 minutes at room temperature. Next, cells were sheared by passing through a 22-gauge syringe needle. DNA was extracted with phenol/chloroform as reported previously (72). Sequence reads from an Illumina HiSeq were converted into barcode counts and deconvoluted by Cellecta, with subsequent merging of gene-target information. The entire final set of sequences consisted of 10,091 uniquely barcoded shRNA targeting 1,287 loci. Most genes (1,110) were targeted by eight barcodes, and the remainder by five to seven barcodes.

Bioinformatics Analysis. We analyzed the read reduction for all shRNA probes across all samples compared with the total reads observed for each shRNA in a simultaneously run plasmid sample (control). We initially analyzed the abundance of barcodes corresponding to survival-critical genes (as identified previously by Cellecta across multiple and diverse cell lines) included as positive controls but found the fold changes of these genes to be subtle, consistent with a general trend across the entire library. On the basis of this, we conjectured that giving greater weight to frequently recurring, highly ranked shRNAs (ranked by fold reduction compared with plasmid) across samples would increase the likelihood for identifying genes critical for leukemic cell survival and/or proliferation due to their recurrence across multiple samples. Barcode counts for each sample were normalized to the number of reads in a simultaneously assessed plasmid sample, and the relative barcode depletion was estimated by calculating the ratio of measured shRNA plasmid input with barcode output counts, adding 20 to numerator and denominator to mitigate high ratios resulting from low read counts. As such, each gene's depletion, also referred to as fold change, is estimated as (plasmid_input gene + 20)/(barcode_count gene + 20). Degrees of depletion were rank partitioned into percentiles for each sample. Candidate genes were prioritized by requiring that at least two of their shRNAs were ranked in the top two-percentile depletion in at least two samples among the set of 12. Sequence reads that did not correspond to known barcodes from the shRNA library were not counted toward the tally for any gene locus. Finally, genes were tallied and ranked for the total number of AML samples within this remaining set. Additional statistical calculations, including ranking of fold reductions, were performed in SAS ver. 9.1 (SAS Institute, Inc.).

IPA

Pathway-associated gene analyses were generated using commercially available software (Qiagen; https://digitalinsights.qiagen.com/products-overview/discovery-insights-portfolio/analysis-and-visualization/qiagen-ipa/). For pathway analysis, metabolite lists were uploaded as exp.log ratio [Kyoto Encyclopedia of Genes and Genomes (KEGG) and Human Metabolome Database (HMDB), identification numbers] into the IPA server. The IPA function Core Analysis/Metabolomics Analysis was used for the enriched pathway identification. In addition, IPA includes an upstream regulator analysis to determine whether the observed metabolic perturbations are associated with a particular upstream regulator. *P* values, calculated from the right-tailed Fisher exact test, reflect whether the number of overlapping metabolites associated with a particular pathway or upstream regulator is greater than expected by chance. For upstream regulator analysis, both direct and indirect relationships between metabolites and their targets were considered. The overall activation/inhibition status of the upstream regulator was determined from the level of consistency in the observed up or down changes of the metabolites. The strength of evidence was statistically represented by *z*-score.

Statistical Methods

Prism 8 (GraphPad) was used to perform all statistical analysis. For the comparisons of two groups, data were presented as mean ± SEM and analyzed by *t* test. For the comparisons of median survival, Kaplan–Meier curves were analyzed by the log-rank (Mantel–Cox) test. Cellular IC_{50} values were calculated by nonlinear regression analysis. $P < 0.05$ was considered to be statistically significant.

Doxycycline-Inducible shRNA Constructs

For initial validation, the two *SIRT5*-targeting shRNAs with the highest depletion during the screening (sh*SIRT5*^{2311} and sh*SIRT5*^{2312}) were inserted into a doxycycline-inducible vector (pRSIT16-U6Tet-sh-CMV-TetR-2A-TagRFP-2A-Puro, Cellecta) containing the wild-type tetracycline repressor (tetR), which blocks transcription unless 100 ng/mL doxycycline is added. Constructs were packaged and used individually for infection. Cells were sorted for RFP-positive cells. For primary cells, the shRNA-induced suppression of *SIRT5* was assessed by measuring mRNA transcripts using SYBR Green– and SIRT5-specific primers (Supplementary Table S6) in a CFX96 Real-Time System (Bio-Rad). For cell lines, the KD of SIRT5 was assayed by immunoblotting.

CRISPR

SIRT5 Guide RNA/Cas9 Expression Vector Construction. The Lenti-CRISPR-v2-PURO plasmid was purchased from Addgene (#52961, a gift from Feng Zhang, Broad Institute, Cambridge, MA; http://n2t.net/addgene:52961; RRID:Addgene_52961; ref. 73). The puromycin-resistant gene was removed and replaced with ZsGreen1 using restriction-enzyme cloning to produce Lenti-CRISPR-v2-ZsGreen. Three 20-bp guide sequences (gRNA-A: 5′-CATCGATGAGC TGCACCGCA-3′, gRNA-B: 5′-GTTCCGACCTTCAGAGGAGC-3′ and gRNA-C: 5′-AAGCACATAGTCATCATCTC-3′) targeting SIRT5 were selected from a published database of predicted high-specificity protospacer adjacent motif (PAM) target sites for human SIRT5. In addition, a nontargeting oligo control was cloned (5′-TGACAT CAATTATTATACAT-3′). Complementary oligos were designed with 5′- and 3′-overhangs for cloning and purchased from Invitrogen. Each pair of oligonucleotides was annealed at a concentration of 10 μmol/L in annealing buffer. The Lenti-CRISPR-v2-ZsGreen plasmid was digested with *Bsm*BI (New England BioLabs) to remove the filler and gel purified. Each pair of oligonucleotides (790 pg) was ligated in the Lenti-CRISPR-v2-ZsGreen vector (50 ng) using QuickLigase and transformed in OneShot chemically competent Stbl3 cells (Invitrogen) using the manufacturer's protocol. Clones were expended in liquid culture,

and the extracted DNA plasmids (Qiagen) were verified by Sanger sequencing. The four plasmids created in this fashion were as follows: Lenti-CRISPR-v2-ZsGreen1-SIRT5-A, Lenti-CRISPR-v2-ZsGreen1-SIRT5-B, Lenti-CRISPR-v2-ZsGreen1-SIRT5-C, and Lenti-CRISPR-v2-ZsGreen1-Control-OLIGO.

Lentivirus Production. Lenti-CRISPR-v2-ZsGreen1-SIRT5 plasmids were transfected as a stoichiometric mixture (21 μg) in HEK293T/17 cells using Lipofectamine 2000 and Plus Reagent (Invitrogen) together with psPAX2 (15 μg) and pVSV-g (10 μg) to generate lentiviral particles. The virus was concentrated with PEG and stored at −80°C.

Generation of SIRT5 Knockout Cell Line. 5×10^5 cells were plated in a 6-well plate in standard media in the presence of polybrene (8 μg/mL) and infected at high MOI. Four days after infection, the cells were sorted for ZsGreen1 expression and expended in culture for 1 week. Subsequently, the cells were single-cell sorted in 96-well plates and cultured in RPMI media for 2 to 3 weeks. When single-cell colonies were formed and covered more than 50% of the well area, the cells were transferred to 12-well plates for expansion. Again, the cells were verified for ZsGreen1 expression, and only pure population clones were further analyzed. The clones obtained in this manner were processed for RNA/DNA extraction and for protein expression analysis. SIRT5 expression was analyzed by qPCR and immunoblot. For all clones negative for SIRT5 expression, fragments of about 800-bp size around each gRNA locus were PCR amplified from genomic DNA, gel purified, and analyzed by Sanger sequencing to confirm genomic DNA editing.

Cell Culture

AML Cell Lines. AML cell lines (Supplementary Table S4) were grown in RPMI1640 medium (Invitrogen) containing 10% FBS, 2 mmol/L L-glutamine, and 100 U/mL penicillin/streptomycin. In the case of OCI-AML5, TF-1, UT-7, M-07e cells, GM-CSF (10 ng/mL) was added to the culture medium. Cell lines were authenticated using the GenePrint 24 Kit (Promega) and DSMZ Online STR Analysis database at the DNA Sequencing Core at the University of Utah (Salt Lake City, UT). All cell lines were confirmed for *Mycoplasma* negativity using the MycoAlert Mycoplasma Detection Kit (Lonza).

Short-term Liquid Culture of Primary AML and CB CD34$^+$ Cells. FACS-sorted RFP$^+$ CD34$^+$ cells were plated at 5×10^3–2×10^4 cells/well in 96-well plates in RPMI supplemented with 10% FBS and cytokines [for AML: CC100, GM-CSF (10 ng/mL), and G-CSF (10 ng/mL); for CB: CC100 only, ± doxycycline (100 ng/mL)], for 3 to 5 days.

Cell Proliferation Assays

Cells were seeded in triplicate in 96-well plates ($5–9 \times 10^3$ cells/well) ± doxycycline (100 ng/mL). Viable cells were measured using CellTiter 96 AQueous One Solution MTS Reagent (Promega) on an Epoch microplate spectrophotometer (BioTek Instruments).

Colony-Forming Assays

AML Cell Lines. Cells were seeded in duplicate at $0.1–0.2 \times 10^3$/dish in MethoCult H4230 (StemCell Technologies) ± 100 ng/mL doxycycline or in the presence and absence of graded concentrations of NRD167. Colonies were counted 7 to 10 days after planting.

Primary AML and CB CD34$^+$ Cells. FACS-sorted RFP$^+$ (AML patient cells: $2–4 \times 10^3$ cells/dish; CB: 1×10^3 cells/dish) were plated in duplicate in MethoCult H4230 with CC100, GM-CSF (10 ng/mL), and G-CSF (10 ng/mL; AML cells) or CC100 only (CB), ± doxycycline (100 ng/mL). For inhibitor studies, nontransduced cells were plated with graded concentrations of NRD167. Colonies were scored after 10 to 15 days. AML colony-forming assays were considered informative if an average of at least 15 colonies/dish was present in the control (no doxycycline).

Mouse BM Cell

Effects of SIRT5 Knockout on Leukemogenicity. Mouse BM cells transduced with leukemia-associated oncogenes (1×10^5 cells/dish) were plated in duplicate in methylcellulose medium without cytokine (Methocult M3231, StemCell Technologies) to detect cytokine-independent CFU-GM colonies.

Effects of SIRT5 Knockout on Physiologic BM Function. Mouse BM cells (2×10^4 cells/dish) from wild-type or *Sirt5*$^{-/-}$ mice were plated in duplicate in complete methylcellulose medium (Methocult M3434, StemCell Technologies). Colonies were scored under an inverted microscope at day 7.

Real-Time Quantitative RT-PCR

RNA was purified with the RNeasy Kit by Qiagen, and cDNA was synthesized with iScript RT Supermix by Bio-Rad. Sirtuin family members 1 to 7 were analyzed with TaqMan Fast Advanced Master Mix (Applied Biosystems) and probe assays from Life Technologies (Supplementary Table S6). Routine monitoring of SIRT5 following induction of shRNA was performed with SsoFast EvaGreen Supermix by Bio-Rad.

Immunoblot Analysis

For immunoblotting, cells were lysed in RIPA lysis buffer containing phosphatase and proteinase inhibitors (Cell Signaling Technology) with freshly added phenylmethylsulfonyl fluoride (PMSF; 2 mmol/L). Protein concentration was measured using the Bradford method. Protein lysates were boiled in Laemmli sample buffer for 5 to 10 minutes and separated on Tris-glycine/SDS-PAGE gels (Bio-Rad), followed by transfer to nitrocellulose membranes. For antibodies used in immunoblotting experiments, see Supplementary Table S7. Images were collected with an Odyssey Fluorescent Imaging System (LI-COR) or a Bio-Rad ChemiDoc and quantified with ImageJ.

Plasmids

Plasmids were obtained from various sources. For complete information, see Supplementary Table S8.

Mitochondrial Protein Fractionation

Cells ($1–5 \times 10^6$) were pelleted, washed, and resuspended in 4 mL sucrose buffer [250 mmol/L sucrose, 1 mmol/L EDTA, 10 mmol/L Tris-HCl (pH 7.4), filtered at 0.2 μm] with PMSF (2 mmol/L) and kept on ice for 15 minutes until the cells expanded as visualized under a microscope. The cell suspension was pulled through an 18-gauge needle and expelled onto the wall of a 50-mL tube through a 26-gauge needle. This process was repeated 15 to 20 times, and break-up of cells was ascertained by inspection under a light microscope. The suspension was then centrifuged at $1,200 \times g$ for 5 minutes at 4°C, and 200 μL of the supernatant was set aside for analysis of total protein. The remaining supernatant was centrifuged at $12,000 \times g$ for 10 minutes at 4°C. Of this supernatant, 200 μL was set aside for analysis of cytosolic protein. The pellets (mitochondria) were washed one to two times with 1 mL sucrose buffer, and then lysed in 2× Laemmli sample buffer, incubated at 100°C for 6 minutes, and stored at −80°C.

Superoxide Dismutase Activity Assay

Superoxide dismutase activity was measured in OCI-AML2 cells 36 hours after the addition of doxycycline with the Superoxide Dismutase (SOD) Colorimetric Activity Kit (Invitrogen) using

1.5×10^7 cells in 400 μL of cold D-PBS. The cell suspension was probe sonicated and centrifuged according to the manufacturer's instructions. Potassium cyanide was added at 2 mmol/L to inactivate SOD1 and SOD3. Results were interpolated from a standard curve in GraphPad Prism and normalized to the results of a Bicinchoninic Acid Protein Assay (Pierce, Thermo Fisher Scientific) run on the same lysate.

Transgenic Mice

C57BL/6 *FLT3-ITD* mice were purchased from The Jackson Laboratory (stock number 011112) and were homozygous for the *FLT3-ITD* mutation. C57BL/6 *SIRT5*$^{-/-}$ mice were kindly given by Dr. Johan Auwerx (Ecole Polytechnique Fédérale de Lausanne, Lausanne, Switzerland). *SIRT5*$^{-/-}$ mice were first crossed with wild-type C57BL/6 mice to generate *SIRT5*$^{+/-}$ mice, which subsequently were bred with homozygous *FLT3-ITD* mice to generate final experimental mice: *FLT3-ITD/Sirt5*$^{+/+}$ and *FLT3-ITD/Sirt5*$^{-/-}$ mice. The experimental mice were monitored daily and blood was analyzed monthly on a HemaTrue Veterinary Hematology Analyzer (Heska). All animal studies were approved by the Institutional Animal Care and Use Committee of the University of Utah (Salt Lake City, UT).

Cell Line Xenografts

NOD.Cg-Prkdcscid Il2rgtm1Wjl/SzJ (NSG) mice (8 weeks old, male, Jackson) were irradiated (200 rad, RadSource 2000, RadSource Technologies), and then injected intravenously with 5×10^5–1×10^6 OCI-AML3 cells or 2×10^6 CMK cells engineered to express doxycycline-inducible sh*SIRT5*$^{2311/2312}$ and luciferase. Doxycycline (2 g/L, with 5% sucrose, Gold Biotechnology) was prepared in 18 MΩ water, filter sterilized, and then delivered as drinking water 18 hours after cell injection and replaced twice weekly. All mice received sulfadimethoxine (0.125 mg/mL, Vet One) in the drinking water throughout the study. Mice were imaged with an IVIS Spectrum *in vivo* imaging system every week, and images were analyzed with Living Image 4.5.4 (PerkinElmer). Luciferin (Gold Biotechnology) was injected intraperitoneally at 150 mg/kg 15 minutes prior to imaging. For CMK cells, mice were randomized between doxycycline and regular water and then maintained on that regimen for 3 weeks. Half of each group was then randomized to cross over to the other regimen, as shown in Fig. 3A. For OCI-AML3 cells, six mice were injected with 0.5–1×10^6 cells/mouse. At 18 hours, mice were randomized between doxycycline and regular water. Mice were considered moribund and euthanized in case of weight loss ≥2 g maintained over consecutive days and in case of other signs of poor health, including minimal responsiveness, hind limb paralysis, or hunched appearance. BM and spleen cells were analyzed for RFP, human CD45-APC (Clone HI30), and mouse CD45-FITC (Clone 30-F11; Tonbo Biosciences) on a BD Biosciences LSRFortessa flow cytometer. Mouse procedures were carried out according to guidelines approved by the Institutional Animal Care and Use Committee at University of Utah (Salt Lake City, UT), protocols 16-11002 and 19-11010 (principal investigator: M.W. Deininger).

Patient-Derived Xenografts

CD34$^+$ cells from a newly diagnosed AML patient were cultured in cytokine-containing medium and treated with vehicle or NRD167 (12.5 or 25 μmol/L) for 72 hours (2.3×10^6 cells per condition). After treatment, cells were harvested and washed once with cold PBS, and then injected via tail vein into 10-week-old sublethally irradiated (2 Gy) male NOD.Cg-Prkdcscid Il2rgtm1Wjl Tg(CMV-IL3,CSF2,KITLG)1Eav/MloySzJ mice (SGM-3, The Jackson Laboratory; five mice per treatment arm). Mice were monitored by bleeding every 3 weeks (except pandemic period) and assessed for human engraftment by flow cytometry using anti-mouse CD45-FITC (clone 30-F11, Tonbo Biosciences) and anti-human CD45-APC (clone HI30, Tonbo Biosciences).

Retroviral Transduction of Mouse BM Cells

Sirt5$^{+/+}$ mice or *Sirt5*$^{-/-}$ littermates were injected with 5-FU (Fresenius Kabi; 100 μg/g of body weight). Four to five days later, BM cells were harvested from 5-FU–primed mice and cultured overnight in DMEM (Invitrogen) supplemented with 15% FBS, 15% WEHI, murine IL3 (7 ng/mL), murine IL6 (12 ng/mL), and murine SCF (56 ng/mL; PeproTech, for all mouse cytokines). Half of BM cells were then transduced with pMSCV-GFP retrovirus for expression of leukemia-associated oncogenes by two rounds of spinoculation with 10 μg/mL polybrene and HEPES (10 mmol/L) at 2,500 rpm for 90 minutes at 32°C. Oncogenes tested were *BCR-ABL1*^{p210}, *FL3-ITD, MLL-AF9, RUNX1-RUNXT1/NRAS*^{G12D}, and *MPL*^{W515L}. Transduced cells were used in colony assays or transplantation models.

BM Transplantation

***BCR-ABL1*^{p210}.** GFP$^+$, lineage-negative, Sca-1$^+$Kit$^+$ cells were sorted from transduced C57BL/6 *Sirt5*$^{+/+}$ or *Sirt5*$^{-/-}$ BM 48 hours after first infection. Five thousand GFP$^+$Lin$^-$Sca-1$^+$Kit$^+$ cells plus 3×10^5 untransduced BM cells from *Sirt5*$^{+/+}$ or *Sirt5*$^{-/-}$ donors, respectively, were injected into lethally irradiated *Sirt5*$^{+/+}$ recipient mice (two doses of 450 rad, 4 hours apart). For maintenance of identical genetic background, all recipients were 6 to11 weeks old and gender-matched *Sirt5*$^{+/+}$ littermates from the same colony. Mice were monitored by daily inspection, weekly body weight measurement, weekly complete blood counts, and weekly FACS for GFP. Moribund animals (see xenograft studies) were sacrificed and subjected to detailed autopsy, FACS analysis, and histology as appropriate.

MLL-AF9. Following transduction, 3×10^5 cells/mouse were injected into lethally irradiated *Sirt5*$^{+/+}$ recipient mice (two doses of 450 rad, 4 hours apart). For maintenance of identical genetic background, all recipients were 6 to 11 weeks old and gender-matched *Sirt5*$^{+/+}$ littermates from the same colony. Mice were monitored as described above. For secondary transplants, 5,000 GFP$^+$Lin$^-$Kit$^+$ cells sorted from the BM of primary recipients were injected into secondary *Sirt5*$^{+/+}$ recipients, with 3×10^5 untransduced BM cells from *Sirt5*$^{+/+}$ or *Sirt5*$^{-/-}$ donors, respectively, for support. Mice were followed as described above for BCR-ABL1^{p210}.

Quantification of Mitochondrial DNA Copy Number

Analysis of mitochondrial DNA copy number was performed by comparing expression of the mitochondrial encoded gene NADH Dehydrogenase 1 (*ND1*) with the nuclear encoded gene Hemoglobin (*HGB*) as described previously (19). Expression data were generated by performing qPCR with 5 ng genomic DNA per reaction, 500 nmol/L target-specific primers for ND1 and HGB (for sequences see Supplementary Table S6), and SsoFast EvaGreen Supermix (Bio-Rad) on a C1000 Thermal Cycler and CFX96 Real-Time System (Bio-Rad). The reaction consisted of 10-minute activation at 95°C, followed by 40 cycles at 95°C for 15 seconds and 95°C for 1 minute. Reactions were set up in triplicate. Relative expression of ND1 was then calculated from the ΔC_t (HGB C_t – ND1 C_t) and expressed as $2^{\Delta C_t}$.

Transmission Electron Microscopy

Mitochondrial morphology was assessed by transmission electron microscopy at the University of Utah Electron Microscopy Core Laboratory (Salt Lake City, UT) following standard procedures.

Measurement of ROS

Following treatment with doxycycline and/or antioxidant compounds, cells were washed with PBS and incubated with 5 μmol/L MitoSOX Red (Thermo Fisher Scientific) for 60 minutes at 37°C. Cells were washed in PBS and suspended in annexin V binding buffer containing 10 mmol/L HEPES/NaOH (pH 7.4), 140 mmol/L NaCl,

and 2.5 mmol/L $CaCl_2$ and incubated with annexin V-APC (BD Biosciences). After 15 minutes, 4,6-diamidino-2-phenylindole (DAPI; Sigma-Aldrich) was added at 2 μg/mL and fluorescence was measured on a LSRFortessa (BD Biosciences) flow cytometer and analyzed with FlowJo analysis software (Treestar; ref. 62).

GSH Measurement

Cells were seeded in duplicate in white, opaque-walled 96-well plates (8×10^3 cells/well) ± doxycycline (100 ng/mL) for 24, 48, and 72 hours. NAD/NADH and GSH were measured using luminescence-based assays according to the manufacturer's instructions (NAD/NADH-Glo, and GSH-Glo, Promega) on a Synergy HT microplate spectrophotometer (BioTek Instruments).

Global Metabolic Profiling

Oxygen consumption and glycolysis of intact cells were measured using XF Cell Mito Stress Test Kit and Glycolysis Stress Test Kit on a Seahorse XFe96 Analyzer (Agilent) at the Metabolic Phenotyping Core Facility at the University of Utah (Salt Lake City, UT) according to the manufacturer's instructions. Briefly, Seahorse XF96 microplates were first coated with 20 μL/well of Cell-TAK adhesive (Corning) at 22.4 μg/mL in 0.1 mol/L $NaHCO_3$ (pH 8.0) for 20 minutes at room temperature to increase adherence of AML cells. Next 1–1.5 × 10^5 cells/well were attached to the plate by centrifugation at 200 × *g* for 3 minutes without brakes. After spinning, cells were rested at 37°C for 30 to 40 minutes in a CO_2-free incubator before analyzing. XF Base medium (DMEM without sodium bicarbonate; Agilent) was used for all experiments. Depending on the experiment, XF base medium was supplemented with either 2 mmol/L glutamine (for glycolytic stress test) or pyruvate (1 mmol/L), glucose (10 mmol/L), and glutamine (2 mmol/L; for Mito Stress test) on the day of assay and adjusted to 7.4 with 1 N NaOH at 37°C. Respiration was measured under basal conditions, with sequential addition of 1 μmol/L oligomycin (ATP synthase inhibitor), 1 μmol/L carbonil-cyanide p-trifluoromethoxyphenylhydrazone (FCCP, mitochondrial oxidative phosphorylation uncoupler), and 0.5 μmol/L rotenone and antimycin A (electron transport chain complex I and III inhibitors). Glycolysis was measured under basal conditions, with sequential addition of 10 mmol/L glucose, 1 μmol/L oligomycin, and 50 mmol/L 2-deoxy-glucose (hexokinase inhibitor).

Steady-state Metabolomics

Cell Culture and Sample Preparation. SIRT5-dependent cell lines (CMK and SKM-1) and SIRT5-independent cell lines (OCI-AML3 and KG1a) expressing doxycycline-sh*SIRT5*$^{2311+2312}$ were harvested after culturing ± doxycycline (100 ng/mL) for 36 and 48 hours, and washed twice in cold PBS. Samples were aliquoted into five 1.5-mL tubes (replicates) with 8–12 × 10^6 cells/tube, and snap-frozen in liquid nitrogen. Cell numbers were equal for each cell line at each time point ± doxycycline. For metabolite extraction, 450 μL of cold 90% methanol solution containing an appropriate amount of internal standard (1 μg of d4-succinic acid) was added to each sample tube. Each tube was vortexed thoroughly, sonicated for 3 minutes, and incubated at −20°C for 1 hour. After incubation, the sample tubes were centrifuged at 20,000 × *g* for 5 minutes at 4°C. The supernatant was transferred from each sample tube into labeled microcentrifuge tubes. A quality control sample was created by removing approximately 15% volume of the collected supernatant from each sample and mixing it in a single tube. Simultaneous to the extraction of samples, process blanks were prepared in the same manner as real sample but substituting deionized water for sample.

Gas Chromatography–Mass Spectrometry Analysis. All gas chromatography–mass spectrometry (GC-MS) analysis was performed with a Waters GCT Premier mass spectrometer fitted with an Agilent 6890 gas chromatograph and a Gerstel MPS2 autosampler. Dried samples were suspended in 40 μL of a 40 mg/mL O-methoxylamine hydrochloride (MOX) in pyridine and incubated for 1 hour at 30°C. To autosampler vials was added 25 μL of this solution; 40 μL of N-methyl-N-trimethylsilyltrifluoracetamide was added automatically via the autosampler and incubated for 60 minutes at 37°C with shaking. After incubation, 3 μL of a fatty acid methyl ester standard (FAMES) solution was added via the autosampler and then 1 μL of the prepared sample was injected to the gas chromatograph inlet in the split mode with the inlet temperature held at 250°C. A 10:1 split ratio was used for analysis. The gas chromatograph had an initial temperature of 95°C for 1 minute, followed by a 40°C/minute ramp to 110°C and a hold time of 2 minutes. This was followed by a second 5°C/minute ramp to 250°C, a third ramp to 350°C, and then a final hold time of 3 minutes. A 30 m Phenomex ZB5–5 MSi column with a 5 m long guard column was employed for chromatographic separation. Helium was used as the carrier gas at 1 mL/minute. Because of the high amounts of several metabolites, the samples were analyzed once more at a 10-fold dilution. Data were collected using MassLynx 4.1 software (Waters). Metabolites were identified, and their peak area was recorded using QuanLynx. These data were transferred to an Excel spreadsheet (Microsoft). Metabolite identity was established using a combination of an in-house metabolite library developed using pure purchased standards and the commercially available NIST library.

LC-MS Analysis. Prior to analysis, samples and process blanks were transferred to PTFE autosampler vials. Quality control samples were tested in four technical replicates, and the order of actual samples was randomized. An Agilent 6550 UPLC-QToF (Agilent Technologies, Inc.) run in both positive and negative modes was used for analysis. Separation was achieved using a Sequant zic-pHILIC 2.1 × 100 mm column (Millipore Sigma) with Phenomenex Krudkatcher (Phenomenex). An initial concentration of 90% ACN (buffer A) and 10% 10 mmol/L ammonium carbonate in ddH_2O (buffer B) was held for 1 minute at a flow rate of 0.3. A was decreased to 20% over 20 minutes and held for 2 minutes. A was returned to starting conditions over 2 minutes, and the system was allowed to re-equilibrate for 6 minutes between runs at a flow rate of 0.4 mL/minute. Data were collected using MassHunter 7.0 software (Agilent). Molecular features were identified using MassHunter Profinder 8.0, and their peak area was recorded using MassHunter Quant 7.0. These data were transferred to an Excel spreadsheet (Microsoft). Metabolite identity was established using a combination of an in-house metabolite library developed using pure purchased standards and the METLIN library. Altered metabolites were identified, and statistical analysis was performed using Mass Profiler Professional (Agilent).

Metabolic Flux

SKM-1 cells expressing doxycycline-sh*SIRT5*$^{2311/2312}$ were cultured in RPMI medium ± 100 ng/mL doxycycline. At 28, 32, or 35 hours after doxycycline addition, cells were spun down and resuspended in either RPMI medium (no L-glutamine, 21870–076, Gibco) supplemented with [$^{13}C_5{}^{15}N_2$]-L-glutamine (final concentration: 2 mmol/L; CNLM-1275-H-0.1, Cambridge Isotope) or RPMI medium (no glucose, 11879–020, Gibco) supplemented with 1,2,3–$^{13}C_3$ glucose (final concentration: 11 mmol/L; 720127; Sigma-Aldrich) ± doxycycline for 1, 4, and 8 hours, for a total time of 36 hours ± doxycycline. Cells were then harvested and washed three times with cold PBS, counted and aliquoted into 1.5-mL tubes with 1–2 × 10^6 cells/tube, four replicates/sample/time point. Cells were then snap-frozen and stored in liquid nitrogen and shipped on dry ice to the University of Colorado (Aurora, CO). Metabolites were extracted from frozen cell pellets at 2 × 10^6 cells/mL of ice-cold lysis/extraction buffer (5:3:2 MeOH:MeCN:H_2O) as described previously (69, 74). Following

centrifugation, samples were randomized, and 10 µL of supernatants were injected into a Thermo Vanquish UHPLC coupled online to a Thermo Q Exactive mass spectrometer operating in positive and negative ion modes (separate runs). Metabolites were separated on a 5-minute C18 gradient as described previously (74). Instrument stability was assessed via injections of technical replicate samples every 10 runs and ensuring a peak area coefficient of variation of <10%. Metabolite assignments and peak area integrations were performed using Maven (Princeton University, Princeton, NJ) in conjunction with the KEGG database following conversion of .raw files to the .mzXML file type using RawConverter. Stable isotope tracing data was plotted in Prism 8 (GraphPad).

Experimental Methods and Materials for Organic Synthesis

All reagents and solvents were of analytic grade and used without further purification as obtained from commercial suppliers. Anhydrous solvents were obtained from a PureSolv-system. Reactions were conducted under an atmosphere of argon or nitrogen whenever anhydrous solvents were used. All reactions were monitored by thin-layer chromatography (TLC) using silica gel–coated plates (analytic SiO2–60, F-254). TLC plates were visualized under UV light and by dipping in either (i) a solution of potassium permanganate (10 g/L), potassium carbonate (67 g/L), and sodium hydroxide (0.83 g/L) in water; (ii) a solution of ninhydrin (3 g/L) in 3% acetic acid in water (v/v); or (iii) a solution of molybdate-phosphoric acid (12.5 g/L) and cerium(IV)sulfate (5 g/L) in 3% conc. sulfuric acid in water (v/v) followed by heating with a heat gun. Vacuum liquid chromatography was performed with silica gel 60 (particle size 15–40 µm). After column chromatography, appropriate fractions were pooled and dried at high vacuum (<2 mbar) for at least 12 hours to give obtained products in high purity (>95%) unless otherwise stated. Evaporation of solvents was carried out under reduced pressure at a temperature below 40°C. UPLC–MS analyses were performed on a Phenomenex Kinetex column (1.7 µmol/L, 50 × 2.10 mm) using a Waters Acquity ultra high–performance liquid chromatography (UPLC) system. Gradient A with eluent I (0.1% HCOOH in H2O) and eluent II (0.1% HCOOH in MeCN) rising linearly from 0% to 95% of II during t = 0.00–5.20 minutes was applied at a flow rate of 0.6 mL/minute. Preparative reverse-phase high-performance liquid chromatography (HPLC) purification was performed on a C18 Phenomenex Luna column (5 µmol/L, 100 Å, 250 × 20 mm) using an Agilent 1260 LC system equipped with a diode array UV detector and an evaporative light scattering detector (ELSD). Gradient B with eluent III (H2O/MeCN/TFA, 95:5:0.1) and eluent IV (0.1% TFA in MeCN) rising linearly from 0% to 95% of IV during t = 5–45 minutes and then isocratically at 95% during t = 45–50 minutes was applied at a flow rate of 20 mL/minute. Analytic HPLC was performed on a C18 Phenomenex Luna column (3 µmol/L, 100 Å, 150 × 4.60 mm) using an Agilent 1100 series system equipped with a diode array UV detector. Gradient C using eluent III and eluent IV, rising linearly from 0% to 95% of IV during t = 5–35 minutes was applied at a flow rate of 1 mL/minute. High-resolution mass spectrometry (HRMS) measurements were recorded either on a maXis G3 quadrupole time-of-flight (TOF) mass spectrometer (Bruker Daltonics) equipped with an electrospray ionization (ESI) source or on an Agilent 1290 UHPLC equipped with a diode array detector and coupled to Agilent 6550 QTOF mass spectrometer operated in positive electrospray or on a Bruker Solarix WR by either matrix assisted laser desorption/ionization, or ESI. Nuclear magnetic resonance (NMR) spectra were recorded either on a Bruker Avance III HD equipped with a cryogenically cooled probe (1H NMR and 13C NMR recorded at 600 and 151 MHz, respectively) or a Bruker Avance III (1H NMR, 13C NMR, and 19F NMR recorded at 400, 101, and 377 MHz, respectively). All spectra were recorded at 298 K unless otherwise stated. Chemical shifts are reported in ppm relative to deuterated solvent as internal standard (ΔH DMSO-d_6 2.50 ppm; ΔC DMSO-d_6 39.52 ppm). Assignments of NMR spectra are based on two-dimensional correlation spectroscopy (COSY, HSQC, and HMBC spectra).

NRE139

The Boc group in **S1** (Supplementary Fig. S10) was removed by iPr$_3$SiH (0.3 mL, 1.5 mmol) and TFA (5 mL, 65.3 mmol) added to a solution of **S1** (870 mg, 1.35 mmol) in CH_2Cl_2 (7.5 mL). The reaction mixture was stirred at ambient temperature for 1.5 hours and was then concentrated *in vacuo*. Excess TFA was removed by coevaporation with CH_2Cl_2/toluene (1:1, 2 × 100 mL), CH_2Cl_2/heptane/CH_3OH (1:1:0.06, 2 × 100 mL), and CH_2Cl_2/CH_3OH (1:0.06, 100 mL), affording an off-white solid, tentatively assigned as the resulting TFA salt (UPLC-MS t_R 1.29 minutes, m/z 544.2; $[M+H]^+$, $C_{27}H_{35}N_5O_4SF^+$ Calcd 544.2), which was used without further purification. A solution of HCl·β-alanine t-butyl ester (50 mg, 0.32 mmol) and iPr$_2$NEt (85 µL, 0.49 mmol) in anhydrous CH_2Cl_2 (8.0 mL) was added dropwise (5 minutes) to a solution of **S2** (Supplementary Fig. S10; 87 mg, 0.31 mmol) in anhydrous CH_2Cl_2 (4.0 mL) at 0°C. The reaction mixture was stirred at 0°C for 10 minutes and was then concentrated under reduced pressure. The crude residue and the TFA salt of the Boc-deprotected derivative of compound **S1** (98 mg, ~0.15 mmol) were dissolved in anhydrous DMF (4.0 mL). Then, iPr$_2$NEt was added (129 µL, 0.56 mmol), and the reaction mixture was stirred overnight at ambient temperature and was then concentrated under reduced pressure. Preparative reverse-phase HPLC purification of the crude residue afforded the desired ester **NRE139** (Supplementary Fig. S10) (37 mg, 17% from **S1**) as a colorless fluffy material after lyophilization. ^{1}H NMR (600 MHz, DMSO-d_6) Δ 10.80 (d, J = 2.4 Hz, 1H, NH_{Indole}), 8.09 (d, J = 8.6 Hz, 1H, $NH_{\alpha,Lys}$), 8.05 (d, J = 7.9 Hz, 1H, $NH_{\alpha,Trp}$), 8.00 (d, J = 7.8 Hz, 1H, $CO_{Trp}NH$), 7.53 (dt, J = 8.5, 2.1 Hz, 1H, $H2_{FPh}$), 7.51–7.47 (m, 2H, $H4_{Indole}$, $H6_{FPh}$), 7.43 (s, 1H, $NH_{\varepsilon,Lys}$), 7.39–7.33 (m, 3H, $H4_{FPh}$, $H5_{FPh}$, $NH(CH_2)_2CO_2Et$), 7.31 (dd, J = 8.1, 0.9 Hz, 1H, $H7_{Indole}$), 7.05 (ddd, J = 8.1, 7.0, 1.1 Hz, 1H, $H6_{Indole}$), 7.01 (d, J = 2.3 Hz, 1H, $H2_{Indole}$), 6.96 (ddd, J = 8.0, 6.9, 1.0 Hz, 1H, $H5_{Indole}$), 4.26–4.21 (m, 1H, $H_{\alpha,Trp}$), 4.13–4.02 (m, 3H, $C\underline{H}_2CH_3$, $H1_{Cyclobutyl}$), 3.76 (td, J = 8.6, 5.5 Hz, 1H, $H_{\alpha,Lys}$), 3.59 (br s, 2H, $C\underline{H}_2CH_2CO_2Et$), 3.20 (br s, 2H, $H_{\varepsilon,Lys}$), 2.90 (m_{ABX}, J = 14.4, 6.9 Hz, 1H, $H_{\beta,Trp,A}$), 2.72 (m_{ABX}, J = 14.4, 6.8 Hz, 1H, $H_{\beta,Trp,B}$), 2.54 (t, J = 6.7 Hz, 2H, $C\underline{H}_2CO_2Et$), 2.13–2.03 (m, 1H, $H2_{Cyclobutyl,A}$), 2.02 – 1.93 (m, 1H, $H2_{Cyclobutyl,B}$), 1.84–1.74 (m, 1H, $H4_{Cyclobutyl,A}$), 1.68–1.60 (m, 1H, $H4_{Cyclobutyl,A}$), 1.59–1.49 (m, 2H, $H3_{Cyclobutyl}$), 1.49–1.27 (m, 4H, $H_{\beta,Lys}$, $H_{\Delta,Lys}$), 1.23–1.13 (m, 4H, $H_{\gamma,Lys,A}$, $CH_2C\underline{H}_3$), 1.05 (ddt, J = 17.0, 12.9, 4.0 Hz, 1H, $H_{\gamma,Lys,B}$). ^{13}C NMR (151 MHz, DMSO) Δ 171.5 (CO_2Et), 170.1 (CO_{Lys}), 169.6 (CO_{Trp}), 161.5 (d, J = 247.7 Hz, $C3_{FPh}$), 158.2 (q, J = 36.9 Hz, CO_{TFA} residual TFA), 143.0 (d, J = 6.6 Hz, $C1_{FPh}$), 135.9 ($C7a_{Indole}$), 131.1 (d, J = 7.9 Hz, $H5_{FPh}$), 127.4 ($C3a_{Indole}$), 123.4 ($C2_{Indole}$), 122.6 (d, J = 3.0 Hz, $C6_{FPh}$), 120.8 ($C6_{Indole}$), 119.3 (d, J = 21.1 Hz, $C4_{FPh}$), 118.4 ($C4_{Indole}$), 118.1 ($C5_{Indole}$), 115.4 (d, J = 290.8 Hz, $CF_{3,TFA}$ residual TFA), 113.6 (d, J = 24.2 Hz, $C2_{FPh}$), 111.1 ($C7_{Indole}$), 109.6 ($C3_{Indole}$), 59.9 ($\underline{C}H_2CH_3$), 56.2 ($C_{\alpha,Lys}$), 53.2 ($C_{\alpha,Trp}$), 43.8 ($C1_{Cyclobutyl}$), 43.3 ($C_{\varepsilon,Lys}$), 38.7 ($\underline{C}H_2CH_2CO_2Et$), 33.6 ($\underline{C}H_2CO_2Et$), 32.6 ($C_{\beta,Lys}$), 30.0 ($C2_{Cyclobutyl}$), 29.9 ($C4_{Cyclobutyl}$), 28.1 ($C_{\Delta,Lys}$), 27.7 ($C_{\beta,Trp}$), 22.5 ($C_{\gamma,Lys}$), 14.6 ($C3_{Cyclobutyl}$), 14.1 ($CH_2\underline{C}H_3$). 19F NMR (376 MHz, DMSO) Δ -74.9 (s, CF_3,TFA), -111.0 (s, 3_{FPh}-F). The peak for C = S was not visible in ^{13}C NMR, presumably due to fast quadrupolar relaxation via the nearby ^{14}N-nuclei. UPLC-MS Tr 1.93 minutes, m/z 703.4 ([M+H]+,$C_{33}H_{44}N_6O_6S_2F^+$ Calcd 703.3); HRMS m/z 703.2745 ([M+H]+, $C_{33}H_{44}N_6O_6S_2F^+$Calcd 703.2742). FPh = 3-fluorophen-1-yl.

Authors' Disclosures

C.C. Mason reports other support from Intermountain Healthcare Foundation and Primary Children's Hospital Foundation, and grants from NIH during the conduct of the study. A.B. Patel reports research

funding from Genentech and American Society of Hematology. J.E. Cox reports grants from NIH/National Institute of Diabetes and Digestive and Kidney Diseases (NIDDK) during the conduct of the study. C.A. Olsen reports grants from Novo Nordisk Foundation during the conduct of the study. M.W. Deininger reports grants from NIH/NCI (R21CA20593601, R01CA254354, and P30-CA042014-24), The V Foundation (T2017-008), Lady Tata Memorial Trust, Leukemia & Lymphoma Society, American Society of Hematology, and NIH (1S10RR026802-01) during the conduct of the study. No disclosures were reported by the other authors.

Disclaimer

The content is solely the responsibility of the authors and does not necessarily represent the official views of the NIH.

Authors' Contributions

D. Yan: Conceptualization, data curation, formal analysis, supervision, investigation, writing–original draft, writing–review and editing. **A. Franzini:** Supervision, investigation, writing–review and editing. **A.D. Pomicter:** Data curation, formal analysis, supervision, investigation, writing–original draft, writing–review and editing. **B.J. Halverson:** Investigation. **O. Antelope:** Investigation. **C.C. Mason:** Formal analysis, investigation, writing–review and editing. **J.M. Ahmann:** Investigation. **A.V. Senina:** Investigation. **N.A. Vellore:** Investigation. **C.L. Jones:** Investigation. **M.S. Zabriskie:** Investigation. **H. Than:** Investigation. **M.J. Xiao:** Investigation. **A. van Scoyk:** Investigation. **A.B. Patel:** Investigation. **P.M. Clair:** Investigation. **W.L. Heaton:** Investigation. **S.C. Owen:** Supervision, methodology. **J.L. Andersen:** Investigation. **C.M. Egbert:** Investigation. **J.A. Reisz:** Data curation, investigation. **A. D'Alessandro:** Data curation, supervision, investigation. **J.E. Cox:** Investigation. **K.C. Gantz:** Investigation. **H.M. Redwine:** Investigation. **S.M. Iyer:** Investigation. **J.S. Khorashad:** Conceptualization, supervision, investigation. **N. Rajabi:** Resources, investigation. **C.A. Olsen:** Resources, supervision, investigation. **T. O'Hare:** Conceptualization, supervision, investigation, writing–original draft, project administration, writing–review and editing. **M.W. Deininger:** Conceptualization, resources, supervision, funding acquisition, writing–original draft, project administration, writing–review and editing.

Acknowledgments

This work was supported by NCI (NIH) grant R21CA20593601 (to M.W. Deininger), R01CA254354 (to M.W. Deininger), The V Foundation for Cancer Research Translational Award T2017-008 (to M.W. Deininger and T. O'Hare), and a Catalyst award from the University of Utah College of Pharmacy. The Cancer Center Support Grant (NCI P30-CA042014) awarded to the Huntsman Cancer Institute at the University of Utah provided pilot project funds and supported shared resources critical to this project. D. Yan is supported by the International Award from the Lady Tata Memorial Trust, United Kingdom. D. Yan and J.S. Khorashad were supported by the Special Fellow Awards from the Leukemia & Lymphoma Society (LLS). C.C. Mason was funded by the Pediatric Cancer Program that is supported by the Intermountain Healthcare and Primary Children's Hospital Foundations, University of Utah, Department of Pediatrics, and the Division of Hematology/Oncology. A.B. Patel was supported by a Research Training Award for Fellows from American Society of Hematology. N. Rajabi was supported by Novo Nordisk Foundation (grant number NNF17OC0029464). C.L. Jones acknowledges funds from LLS and American Cancer Society. A. D'Alessandro was supported by funds from the Boettcher Webb-Waring Investigator Award, RM1GM131968 by the National Institute of General and Medical Sciences, and R01HL146442 by the National Heart, Lung and Blood Institute. The authors thank Benjamin C. Brown (University of Colorado, Aurora, CO) for technical assistance with metabolomics analyses. They also thank the Metabolic Phenotyping Core Facility at the University of Utah for the assistance with the experiments. This work was supported by the University of Utah Flow Cytometry Facility in addition to the NCI through Award Number 5P30CA042014–24 and the National Center for Research Resources of the NIH under Award Number 1S10RR026802–01. Research reported in this publication utilized the High-Throughput Genomics and Bioinformatic Analysis Shared Resource at the University of Utah Huntsman Cancer Institute, supported by the NCI of the NIH under Award Number P30CA042014. Claire Davis, HCI Communications, assisted with illustrations. The authors thank Dr. Dennis Winge (Division of Hematologic and Hematologic Malignancies, University of Utah, Salt Lake City, UT), Dr. Jared Rutter (Department of Biochemistry, University of Utah, Salt Lake City, UT, and Howard Hughes Medical Institute, Chevy Chase, MD), Dr. David Lombard (Department of Pathology, University of Michigan, Ann Arbor, MI), and Dr. Hening Lin (Department of Chemistry, Cornell University, New York, NY, and Howard Hughes Medical Institute, Chevy Chase, MD) for thoughtful discussion and feedback.

Received September 18, 2020; revised January 19, 2021; accepted March 5, 2021; published first April 10, 2021.

REFERENCES

1. Burnett A, Wetzler M, Lowenberg B. Therapeutic advances in acute myeloid leukemia. J Clin Oncol 2011;29:487–94.
2. Rai KR, Holland JF, Glidewell OJ, Weinberg V, Brunner K, Obrecht JP, et al. Treatment of acute myelocytic leukemia: a study by cancer and leukemia group B. Blood 1981;58:1203–12.
3. Yates J, Glidewell O, Wiernik P, Cooper MR, Steinberg D, Dosik H, et al. Cytosine arabinoside with daunorubicin or adriamycin for therapy of acute myelocytic leukemia: a CALGB study. Blood 1982;60:454–62.
4. Lo-Coco F, Avvisati G, Vignetti M, Thiede C, Orlando SM, Iacobelli S, et al. Retinoic acid and arsenic trioxide for acute promyelocytic leukemia. N Engl J Med 2013;369:111–21.
5. Yang X, Sexauer A, Levis M. Bone marrow stroma-mediated resistance to FLT3 inhibitors in FLT3-ITD AML is mediated by persistent activation of extracellular regulated kinase. Br J Haematol 2014;164:61–72.
6. Dugan J, Pollyea D. Enasidenib for the treatment of acute myeloid leukemia. Expert Rev Clin Pharmacol 2018;11:755–60.
7. Stein EM, DiNardo CD, Pollyea DA, Fathi AT, Roboz GJ, Altman JK, et al. Enasidenib in mutant IDH2 relapsed or refractory acute myeloid leukemia. Blood 2017;130:722–31.
8. Amatangelo MD, Quek L, Shih A, Stein EM, Roshal M, David MD, et al. Enasidenib induces acute myeloid leukemia cell differentiation to promote clinical response. Blood 2017;130:732–41.
9. Stone RM, Mandrekar SJ, Sanford BL, Laumann K, Geyer S, Bloomfield CD, et al. Midostaurin plus chemotherapy for acute myeloid leukemia with a FLT3 mutation. N Engl J Med 2017;377:454–64.
10. Stone RM, Larson RA, Dohner H. Midostaurin in FLT3-mutated acute myeloid leukemia. N Engl J Med 2017;377:1903.
11. DiNardo CD, Pratz K, Pullarkat V, Jonas BA, Arellano M, Becker PS, et al. Venetoclax combined with decitabine or azacitidine in treatment-naive, elderly patients with acute myeloid leukemia. Blood 2019;133:717.
12. DiNardo CD, Stein EM, de Botton S, Roboz GJ, Altman JK, Mims AS, et al. Durable remissions with ivosidenib in IDH1-mutated relapsed or refractory AML. N Engl J Med 2018;378:2386–98.
13. Pollyea DA, Stevens BM, Jones CL, Winters A, Pei S, Minhajuddin M, et al. Venetoclax with azacitidine disrupts energy metabolism and targets leukemia stem cells in patients with acute myeloid leukemia. Nat Med 2018;24:1859–66.
14. Nechiporuk T, Kurtz SE, Nikolova O, Liu T, Jones CL, D'Alessandro A, et al. The TP53 apoptotic network is a primary mediator of resistance to BCL2 inhibition in AML cells. Cancer Discov 2019;9:910–25.
15. Chen X, Glytsou C, Zhou H, Narang S, Reyna DE, Lopez A, et al. Targeting mitochondrial structure sensitizes acute myeloid leukemia to venetoclax treatment. Cancer Discov 2019;9:890–909.

16. Hanahan D, Weinberg RA. Hallmarks of cancer: the next generation. Cell 2011;144:646–74.
17. Warburg O, Wind F, Negelein E. The metabolism of tumors in the body. J Gen Physiol 1927;8:519–30.
18. Vander Heiden MG, Cantley LC, Thompson CB. Understanding the Warburg effect: the metabolic requirements of cell proliferation. Science 2009;324:1029–33.
19. Sriskanthadevan S, Jeyaraju DV, Chung TE, Prabha S, Xu W, Skrtic M, et al. AML cells have low spare reserve capacity in their respiratory chain that renders them susceptible to oxidative metabolic stress. Blood 2015;125:2120–30.
20. Molina JR, Sun Y, Protopopova M, Gera S, Bandi M, Bristow C, et al. An inhibitor of oxidative phosphorylation exploits cancer vulnerability. Nat Med 2018;24:1036–46.
21. Fenouille N, Bassil CF, Ben-Sahra I, Benajiba L, Alexe G, Ramos A, et al. The creatine kinase pathway is a metabolic vulnerability in EVI1-positive acute myeloid leukemia. Nat Med 2017;23:301–13.
22. Hattori A, Tsunoda M, Konuma T, Kobayashi M, Nagy T, Glushka J, et al. Cancer progression by reprogrammed BCAA metabolism in myeloid leukaemia. Nature 2017;545:500–4.
23. Matre P, Velez J, Jacamo R, Qi Y, Su X, Cai T, et al. Inhibiting glutaminase in acute myeloid leukemia: metabolic dependency of selected AML subtypes. Oncotarget 2016;7:79722–35.
24. Gallipoli P, Giotopoulos G, Tzelepis K, Costa ASH, Vohra S, Medina-Perez P, et al. Glutaminolysis is a metabolic dependency in FLT3(ITD) acute myeloid leukemia unmasked by FLT3 tyrosine kinase inhibition. Blood 2018;131:1639–53.
25. Skrtic M, Sriskanthadevan S, Jhas B, Gebbia M, Wang X, Wang Z, et al. Inhibition of mitochondrial translation as a therapeutic strategy for human acute myeloid leukemia. Cancer Cell 2011;20:674–88.
26. Gregory MA, D'Alessandro A, Alvarez-Calderon F, Kim J, Nemkov T, Adane B, et al. ATM/G6PD-driven redox metabolism promotes FLT3 inhibitor resistance in acute myeloid leukemia. Proc Natl Acad Sci U S A 2016;113:E6669–E78.
27. Gregory MA, Nemkov T, Reisz JA, Zaberezhnyy V, Hansen KC, D'Alessandro A, et al. Glutaminase inhibition improves FLT3 inhibitor therapy for acute myeloid leukemia. Exp Hematol 2018;58:52–8.
28. Lagadinou ED, Sach A, Callahan K, Rossi RM, Neering SJ, Minhajuddin M, et al. BCL-2 inhibition targets oxidative phosphorylation and selectively eradicates quiescent human leukemia stem cells. Cell Stem Cell 2013;12:329–41.
29. Pusapati RV, Daemen A, Wilson C, Sandoval W, Gao M, Haley B, et al. mTORC1-dependent metabolic reprogramming underlies escape from glycolysis addiction in cancer cells. Cancer Cell 2016;29:548–62.
30. Cacace A, Sboarina M, Vazeille T, Sonveaux P. Glutamine activates STAT3 to control cancer cell proliferation independently of glutamine metabolism. Oncogene 2017;36:2074–84.
31. Amoedo ND, Obre E, Rossignol R. Drug discovery strategies in the field of tumor energy metabolism: Limitations by metabolic flexibility and metabolic resistance to chemotherapy. Biochim Biophys Acta Bioenerg 2017;1858:674–85.
32. Nakagawa T, Guarente L. SnapShot: sirtuins, NAD, and aging. Cell Metab 2014;20:192–192.e1.
33. Hirschey MD, Zhao Y. Metabolic regulation by lysine malonylation, succinylation and glutarylation. Mol Cell Proteomics 2015; 14:2308–15.
34. Park J, Chen Y, Tishkoff DX, Peng C, Tan M, Dai L, et al. SIRT5-mediated lysine desuccinylation impacts diverse metabolic pathways. Mol Cell 2013;50:919–30.
35. Tan M, Peng C, Anderson KA, Chhoy P, Xie Z, Dai L, et al. Lysine glutarylation is a protein posttranslational modification regulated by SIRT5. Cell Metab 2014;19:605–17.
36. Du J, Zhou Y, Su X, Yu JJ, Khan S, Jiang H, et al. Sirt5 is a NAD-dependent protein lysine demalonylase and desuccinylase. Science 2011;334:806–9.
37. Rardin MJ, He W, Nishida Y, Newman JC, Carrico C, Danielson SR, et al. SIRT5 regulates the mitochondrial lysine succinylome and metabolic networks. Cell Metab 2013;18:920–33.
38. Nishida Y, Rardin MJ, Carrico C, He W, Sahu AK, Gut P, et al. SIRT5 regulates both cytosolic and mitochondrial protein malonylation with glycolysis as a major target. Mol Cell 2015;59:321–32.
39. Bringman-Rodenbarger LR, Guo AH, Lyssiotis CA, Lombard DB. Emerging roles for SIRT5 in metabolism and cancer. Antioxid Redox Signal 2018;28:677–90.
40. Carrico C, Meyer JG, He W, Gibson BW, Verdin E. The mitochondrial acylome emerges: proteomics, regulation by sirtuins, and metabolic and disease implications. Cell Metab 2018;27:497–512.
41. Yu J, Sadhukhan S, Noriega LG, Moullan N, He B, Weiss RS, et al. Metabolic characterization of a Sirt5 deficient mouse model. Sci Rep 2013;3:2806.
42. Liu L, Peritore C, Ginsberg J, Shih J, Arun S, Donmez G. Protective role of SIRT5 against motor deficit and dopaminergic degeneration in MPTP-induced mice model of Parkinson's disease. Behav Brain Res 2015;281:215–21.
43. Wang G, Meyer JG, Cai W, Softic S, Li ME, Verdin E, et al. Regulation of UCP1 and mitochondrial metabolism in brown adipose tissue by reversible succinylation. Mol Cell 2019;74:844–57.
44. Boylston JA, Sun J, Chen Y, Gucek M, Sack MN, Murphy E. Characterization of the cardiac succinylome and its role in ischemia-reperfusion injury. J Mol Cell Cardiol 2015;88:73–81.
45. Hershberger KA, Abraham DM, Martin AS, Mao L, Liu J, Gu H, et al. Sirtuin 5 is required for mouse survival in response to cardiac pressure overload. J Biol Chem 2017;292:19767–81.
46. Roecklein BA, Torok-Storb B. Functionally distinct human marrow stromal cell lines immortalized by transduction with the human papilloma virus E6/E7 genes. Blood 1995;85:997–1005.
47. Garrido SM, Appelbaum FR, Willman CL, Banker DE. Acute myeloid leukemia cells are protected from spontaneous and drug-induced apoptosis by direct contact with a human bone marrow stromal cell line (HS-5). Exp Hematol 2001;29:448–57.
48. Eiring AM, Page BD, Kraft IL, Mason CC, Vellore NA, Resetca D, et al. Combined STAT3 and BCR-ABL1 inhibition induces synthetic lethality in therapy-resistant chronic myeloid leukemia. Leukemia 2015;29:586–97.
49. Chatzispyrou IA, Held NM, Mouchiroud L, Auwerx J, Houtkooper RH. Tetracycline antibiotics impair mitochondrial function and its experimental use confounds research. Cancer Res 2015;75:4446–9.
50. Moullan N, Mouchiroud L, Wang X, Ryu D, Williams EG, Mottis A, et al. Tetracyclines disturb mitochondrial function across eukaryotic models: a call for caution in biomedical research. Cell Rep 2015;10:1681–91.
51. Wallace JA, Kagele DA, Eiring AM, Kim CN, Hu R, Runtsch MC, et al. miR-155 promotes FLT3-ITD-induced myeloproliferative disease through inhibition of the interferon response. Blood 2017;129:3074–86.
52. Polletta L, Vernucci E, Carnevale I, Arcangeli T, Rotili D, Palmerio S, et al. SIRT5 regulation of ammonia-induced autophagy and mitophagy. Autophagy 2015;11:253–70.
53. Olgun A, Akman S. Mitochondrial DNA-deficient models and aging. Ann N Y Acad Sci 2007;1100:241–5.
54. Wang YQ, Wang HL, Xu J, Tan J, Fu LN, Wang JL, et al. Sirtuin5 contributes to colorectal carcinogenesis by enhancing glutaminolysis in a deglutarylation-dependent manner. Nat Commun 2018;9:545.
55. Greene KS, Lukey MJ, Wang X, Blank B, Druso JE, Lin MJ, et al. SIRT5 stabilizes mitochondrial glutaminase and supports breast cancer tumorigenesis. Proc Natl Acad Sci U S A 2019;116:26625–32.
56. Jacque N, Ronchetti AM, Larrue C, Meunier G, Birsen R, Willems L, et al. Targeting glutaminolysis has antileukemic activity in acute myeloid leukemia and synergizes with BCL-2 inhibition. Blood 2015; 126:1346–56.
57. Maurer B, Rumpf T, Scharfe M, Stolfa DA, Schmitt ML, He W, et al. Inhibitors of the NAD(+)-dependent protein desuccinylase and demalonylase Sirt5. ACS Med Chem Lett 2012;3:1050–3.
58. Rajabi N, Auth M, Troelsen KR, Pannek M, Bhatt DP, Fontenas M, et al. Mechanism-based inhibitors of the human sirtuin 5 deacylase: structure-activity relationship, biostructural, and kinetic insight. Angew Chem Int Ed Engl 2017;56:14836–41.

59. Banks CJ, Andersen JL. Mechanisms of SOD1 regulation by post-translational modifications. Redox Biol 2019;26:101270.
60. Banks CJ, Rodriguez NW, Gashler KR, Pandya RR, Mortenson JB, Whited MD, et al. Acylation of superoxide dismutase 1 (SOD1) at K122 governs SOD1-mediated inhibition of mitochondrial respiration. Mol Cell Biol 2017;37:e00354–17.
61. Tao R, Coleman MC, Pennington JD, Ozden O, Park SH, Jiang H, et al. Sirt3-mediated deacetylation of evolutionarily conserved lysine 122 regulates MnSOD activity in response to stress. Mol Cell 2010;40:893–904.
62. Starkov AA. An update on the role of mitochondrial alpha-ketoglutarate dehydrogenase in oxidative stress. Mol Cell Neurosci 2013;55:13–6.
63. Jones CL, Stevens BM, D'Alessandro A, Culp-Hill R, Reisz JA, Pei S, et al. Cysteine depletion targets leukemia stem cells through inhibition of electron transport complex II. Blood 2019;134:389–94.
64. Li F, He X, Ye D, Lin Y, Yu H, Yao C, et al. NADP(+)-IDH mutations promote hypersuccinylation that impairs mitochondria respiration and induces apoptosis resistance. Mol Cell 2015;60:661–75.
65. Zhou L, Wang F, Sun R, Chen X, Zhang M, Xu Q, et al. SIRT5 promotes IDH2 desuccinylation and G6PD deglutarylation to enhance cellular antioxidant defense. EMBO Rep 2016;17:811–22.
66. Liu B, Che W, Zheng C, Liu W, Wen J, Fu H, et al. SIRT5: a safeguard against oxidative stress-induced apoptosis in cardiomyocytes. Cell Physiol Biochem 2013;32:1050–9.
67. Chyla B, Daver N, Doyle K, McKeegan E, Huang X, Ruvolo V, et al. Genetic biomarkers of sensitivity and resistance to venetoclax monotherapy in patients with relapsed acute myeloid leukemia. Am J Hematol 2018;93:E202–5.
68. Konopleva M, Pollyea DA, Potluri J, Chyla B, Hogdal L, Busman T, et al. Efficacy and biological correlates of response in a phase II study of venetoclax monotherapy in patients with acute myelogenous leukemia. Cancer Discov 2016;6:1106–17.
69. Jones CL, Stevens BM, D'Alessandro A, Reisz JA, Culp-Hill R, Nemkov T, et al. Inhibition of amino acid metabolism selectively targets human leukemia stem cells. Cancer Cell 2018;34:724–40.
70. Li M, Chiang YL, Lyssiotis CA, Teater MR, Hong JY, Shen H, et al. Non-oncogene addiction to SIRT3 plays a critical role in lymphomagenesis. Cancer Cell 2019;35:916–31.
71. Trub AG, Hirschey MD. Reactive acyl-CoA species modify proteins and induce carbon stress. Trends Biochem Sci 2018;43:369–79.
72. Khorashad JS, Eiring AM, Mason CC, Gantz KC, Bowler AD, Redwine HM, et al. shRNA library screening identifies nucleocytoplasmic transport as a mediator of BCR-ABL1 kinase-independent resistance. Blood 2015;125:1772–81.
73. Sanjana NE, Shalem O, Zhang F. Improved vectors and genome-wide libraries for CRISPR screening. Nat Methods 2014;11:783–4.
74. Nemkov T, Reisz JA, Gehrke S, Hansen KC, D'Alessandro A. High-throughput metabolomics: isocratic and gradient mass spectrometry-based methods. Methods Mol Biol 2019;1978:13–26.